the plant journal

SEB SOCIETY FOR EXPERIMENTAL BIOLOGY

The Plant Journal (2024) doi: 10.1111/tpj.16760

A complex receptor locus confers responsiveness to necrosis and ethylene-inducing like peptides in *Brassica napus*

Hicret Asli Yalcin[1,2], Catherine N. Jacott[1,3], Ricardo Humberto Ramirez-Gonzalez[1,4], Burkhard Steuernagel[1], Gurpinder Singh Sidhu[1], Rachel Kirby[1], Emma Verbeek[1], Henk-jan Schoonbeek[1,5], Christopher J. Ridout[1] and Rachel Wells[1,*]

[1]*John Innes Centre, Norwich Research Park, Colney Lane, Norwich NR4 7UH, UK,*
[2]*TUBITAK Marmara Research Centre, Life Sciences, TUBITAK, Gebze, Kocaeli 41470, Türkiye,*
[3]*Department of Microbiology, Faculty of Biology, University of Seville, Seville, Spain,*
[4]*Genomics England, One Canada Square, London E14 5AB, UK, and*
[5]*University of East Anglia, Norwich Research Park, Norwich NR4 7TJ, UK*

Received 17 November 2023; revised 2 March 2024; accepted 27 March 2024.
*For correspondence (e-mail rachel.wells@jic.ac.uk).

SUMMARY

Brassica crops are susceptible to diseases which can be mitigated by breeding for resistance. MAMPs (microbe-associated molecular patterns) are conserved molecules of pathogens that elicit host defences known as pattern-triggered immunity (PTI). Necrosis and Ethylene-inducing peptide 1-like proteins (NLPs) are MAMPs found in a wide range of phytopathogens. We studied the response to BcNEP2, a representative NLP from *Botrytis cinerea*, and showed that it contributes to disease resistance in *Brassica napus*. To map regions conferring NLP response, we used the production of reactive oxygen species (ROS) induced during PTI across a population of diverse *B. napus* accessions for associative transcriptomics (AT), and bulk segregant analysis (BSA) on DNA pools created from a cross of NLP-responsive and non-responsive lines. *In silico* mapping with AT identified two peaks for NLP responsiveness on chromosomes A04 and C05 whereas the BSA identified one peak on A04. BSA delimited the region for NLP-responsiveness to 3 Mbp, containing ~245 genes on the Darmor-*bzh* reference genome and four co-segregating KASP markers were identified. The same pipeline with the ZS11 genome confirmed the highest-associated region on chromosome A04. Comparative BLAST analysis revealed unannotated clusters of receptor-like protein (RLP) homologues on ZS11 chromosome A04. However, no specific RLP homologue conferring NLP response could be identified. Our results also suggest that *BR-SIGNALLING KINASE1* may be involved with modulating the NLP response. Overall, we demonstrate that responsiveness to NLP contributes to disease resistance in *B. napus* and define the associated genomic location. These results can have practical application in crop improvement.

Keywords: NEP1-like proteins, NLP-responsiveness, disease resistance, BSK1, *Brassica napus*, oilseed rape, *Arabidopsis thaliana*, ROS, RLPs.

INTRODUCTION

Necrosis- and ethylene-inducing like proteins (NLPs) are a superfamily of proteins widely found in bacteria, fungi and oomycetes (Seidl & Van den Ackerveken, 2019). NLPs can be present in microorganisms that are plant-pathogens but also occur in non-pathogenic taxa suggesting their role is not limited to virulence in plants (Bhatti et al., 2017; Tekaia & Latgé, 2005). NLPs can contain a microbe-associated molecular pattern (MAMP) motif that activates pattern-triggered immunity (PTI) in plants leading to defence gene induction, production of reactive oxygen species (ROS) and other protective mechanisms. Recognition of the *Botrytis cinerea* necrosis and ethylene-inducing like peptide 2 (BcNEP2) by RECEPTOR-LIKE PROTEIN 23 (AtRLP23) contributes to some resistance against *B. cinerea* in *Arabidopsis thaliana* (Ono et al., 2020). In translational research studies, silencing of *BcNEP2* in *B. cinerea* and its corresponding homologue *SsNEP2* in *Sclerotinia sclerotiorum* by dsRNA resulted in a significant reduction of lesion size in *B. napus* (McLoughlin et al., 2018). However, BcNEP2-responsiveness could not be associated with resistance to *B. cinerea* in 12 *B. napus* accessions, possibly because of

their diverse genetic backgrounds and the limited extent of the study (Schoonbeek et al., 2022).

Other MAMPs, including chitin, flagellin and elongation factor Tu (EF-Tu), are well-studied in the Brassicaceae. Short epitopes of EF-Tu (elf18) induce PTI in the Brassicaceae whereas flagellin (flg22) and chitin induce PTI in Brassicaceae and many other plant species. MAMPs are recognised by pattern recognition receptors (PRRs), which include receptor-like kinases (RLKs) and receptor-like proteins (RLPs), which may interact with co-receptors to activate defences. In Arabidopsis, response to NLPs is conferred by RLP23 which forms a complex with the leucine-rich repeat (LRR) receptor kinase, SOBIR1 and recruits a second (LRR) receptor kinase, BAK1, into a complex upon ligand binding (Albert et al., 2015). The LRR-RLK protein family XII includes the PRRs FLAGELLIN SENSITIVE 2 (FLS2) and ELONGATION FACTOR (EF)-Tu RECEPTOR (EFR) in Arabidopsis which respectively recognise flg22 and elf18 (Felix et al., 1999; Gómez-Gómez & Boller, 2000; Kunze et al., 2004; Zipfel et al., 2006). Perception of flg22 by the PRR FLAGELLIN SENSITIVE 2 (FLS2) is a quantitative trait with extensive variation in the Brassicaceae resulting mostly from variation in receptor protein abundance (Vetter et al., 2012). However, perception by PRRs is largely MAMP-specific and variation in response can arise from differences in the receptor protein-coding regions, transcriptional regulation, post-translational modification or differential interaction with co-receptors (Vetter et al., 2016). Also, PRRs typically interact with co-receptors which can provide another level of response variation. For example, the FLS2 receptor physically associates with a co-receptor BSK1 in Arabidopsis during the activation of immunity (Shi et al., 2013). However, the role of BSK1 in NLP perception is not known.

The Brassicaceae comprises 338 genera and more than 3709 species (Schmidt et al., 2001). Six species of major agricultural and horticultural importance in the genus *Brassica* are defined by their genome arrangement (A, B or C) for diploid species, *B. rapa* (AA), *B. nigra* (BB) and *B. oleracea* (CC), that are hybridised in the allotetraploid (amphidiploid) species, *B. juncea* (AABB), *B. napus* (AACC) and *B. carinata* (BBCC) (commonly referred as polyploids). The subject of this study, *B. napus*, is the most important temperate oilseed crop with a production close to 70 million tonnes (Raboanatahiry et al., 2021). *Brassica napus* is affected by pathogens which affect yield and quality of the crop. We previously used *B. cinerea* as a model pathogen with extensive resources to translate disease resistance research from Arabidopsis to *B. napus*. We showed that some *B. napus* accessions could recognise NLPs from various crop pathogens such as *B. cinerea* (BcNEP1 and BcNEP2), *Verticillium longisporum* (VlNLP1), *Leptosphaeria maculans* (LmNLP1), *Alternaria brassicicola* (AbNLP2) and also *Hyaloperonospora arabidopsidis* (HaNLP3) (Schoonbeek et al., 2022).

The polyploid nature of the *B. napus* genome results in multiple homologues of candidate receptor and co-receptor genes involved in NLP responsiveness when compared to Arabidopsis (Schoonbeek et al., 2022). However, the bioinformatics resources for gene identification are well-advanced for *B. napus* including the availability of two reference genomes, ZS11 (Song et al., 2020) and Darmor-*bzh* (Chalhoub et al., 2014). Genome-wide association studies (GWAS) and associative transcriptomics (AT) involve associating single nucleotide polymorphisms (SNPs) in genomes or transcriptomes respectively with polymorphic traits in genetically diverse accessions and have been used to identify candidate resistance gene loci for *S. sclerotiorum* (Sclerotinia stem rot), *Plasmodiophora brassicae* (clubroot) and *Pyrenopeziza brassicae* (light leaf spot) in *B. napus* (Dakouri et al., 2021; Fell et al., 2023; Roy et al., 2021).

Bulked segregant analysis (BSA) is used for identifying genetic markers for specific target loci (Michelmore et al., 1991). BSA can enable candidate genes to be identified quickly from any segregating population (Zou et al., 2016) with NGS-enabled protocols such as RNA-Seq (Trick et al., 2012) or whole-genome re-sequencing (Tudor et al., 2020). Many agronomically important traits have been investigated using BSA with different crop species including *Oryza sativa, Triticum aestivum L.* and *B. napus* (Ramirez-Gonzalez, Segovia, et al., 2015; Takagi et al., 2013; Tudor et al., 2020; Wang et al., 2016).

Our study is based on the hypothesis that NLP responsiveness contributes to disease resistance in *B. napus* in a similar manner to that in Arabidopsis. To address this, we created a mapping population from NLP-responsive and non-responsive lines to test resistance against *B. cinerea*. To localise the candidate NLP receptor and potential co-receptors, we used a combination of AT with a *B. napus* diversity set and a more targeted BSA approach from pools of NLP-responding and non-responding progeny lines of the mapping population. Our strategy and results have potential applications in improving disease resistance in *B. napus*.

RESULTS

Associative Transcriptomics identifies regions associated with NLP-responsiveness on chromosomes A04 and C05

From the diversity set, only 12 out of 189 *B. napus* accessions responded to BcNEP2 (Table S1). Since the response trait is qualitative it can be represented as binary values (1 or 0, for responding and non-responding genotypes, respectively) (Figure 1b; Table S2). For the 12 lines that do respond, quantitative variation is observed in the level of ROS production (Figure 1b).

AT analysis using binary values indicated two major peaks on chromosomes A04 and C05 (Figure 1a,c).

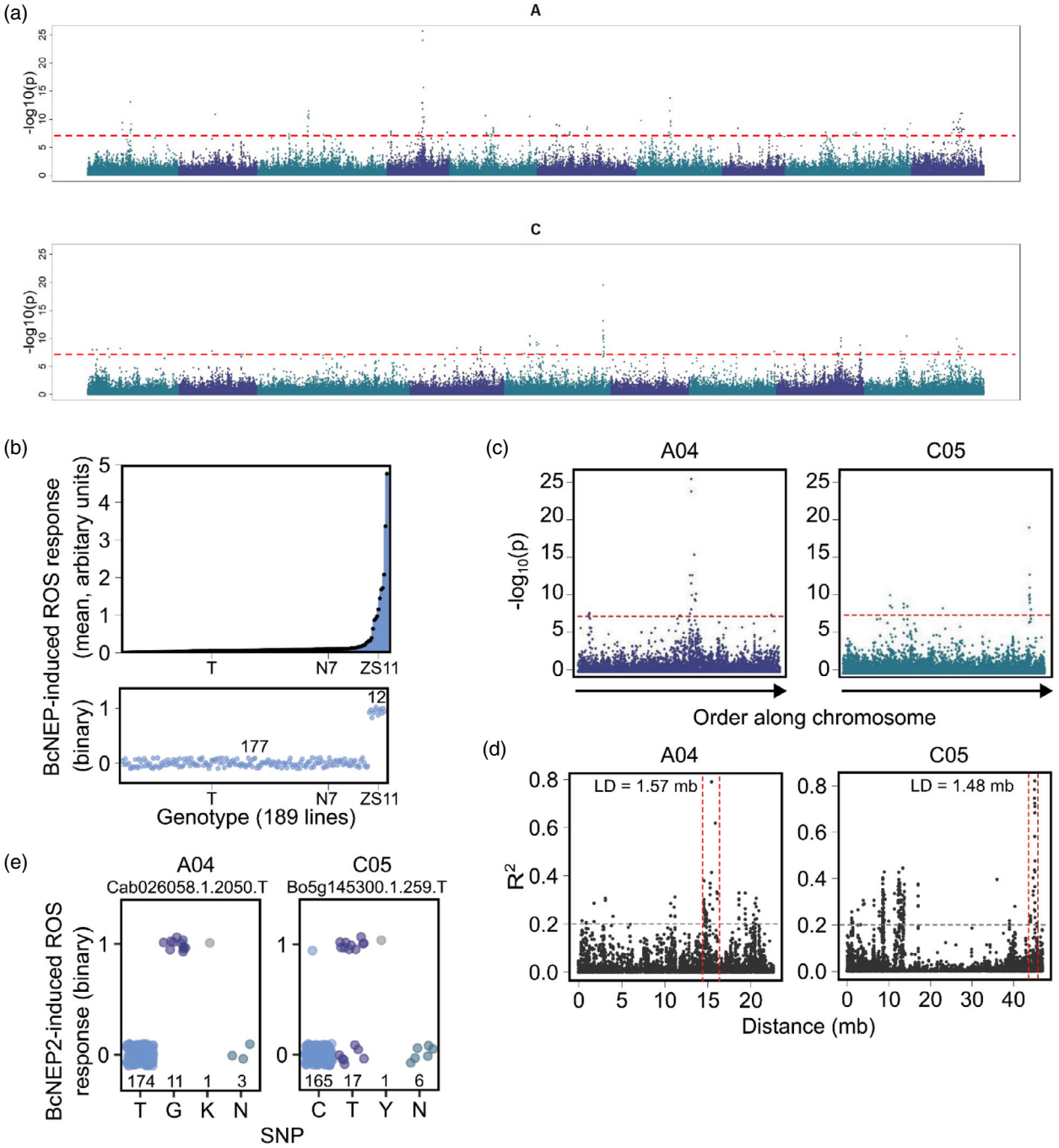

Figure 1. Associative Transcriptomic analysis of BcNEP2-induced ROS production in 191 *B. napus* genotypes.
(a) Manhattan plots showing marker-trait association for binary ROS production to BcNEP2. Red line indicates FDR <0.05.
(b) Mean (calculated using *eemeans* package in R) and binary ROS production of *B. napus* genotypes to BcNEP2. Reference genotypes Tapidor (T), Ningyou 7 (N7) and Zhongshuang11 (ZS11) are indicated.
(c) Manhattan plots showing marker-trait association for binary ROS production. The *x*-axis indicates SNP location by order along chromosome; the *y*-axis indicates the $-\log10(P)$ (*P*-value). Red lines indicate FDR <0.05.
(d) Linkage disequilibrium of the highest associating marker from peaks on chromosome A04 (Cab026058.1.2050.T) and C05 (Bo5g145300.1.256.T). Grey line indicates R^2 value of 0.2, and red lines indicate the area of LD.
(e) Segregation of BcNEP2-induced ROS production in the *B. napus* genotypes of Cab026058.1.2050.T (A04) and Bo5g145300.1.256.T (C05).

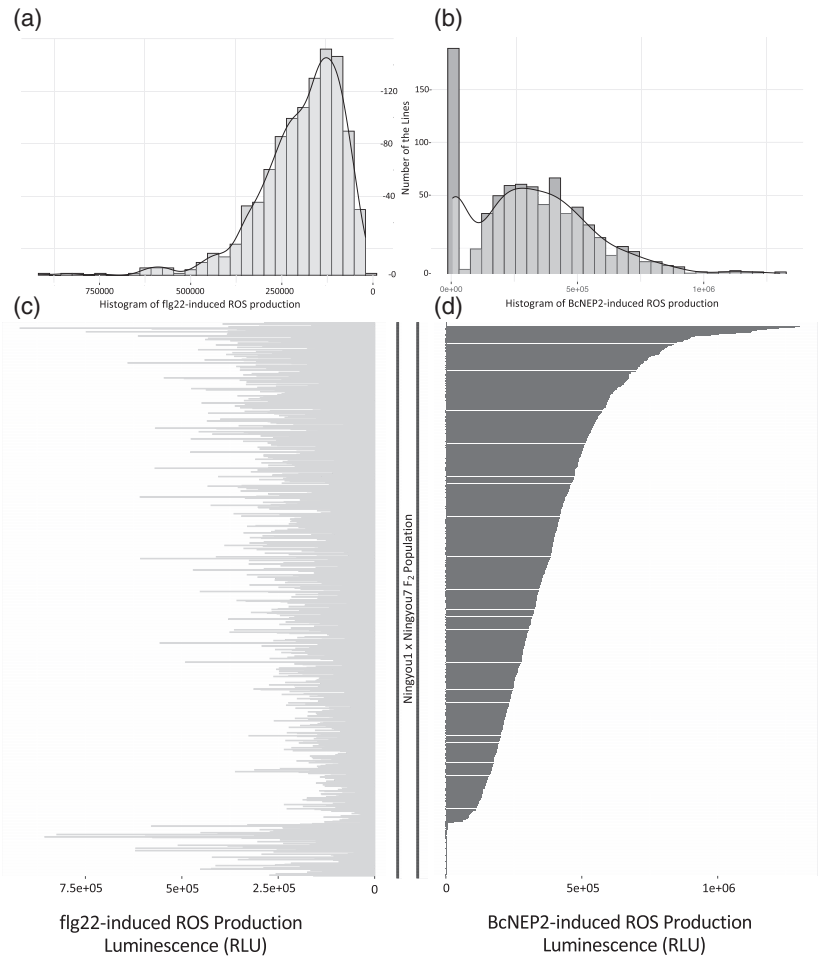

Figure 2. Phenotype data of each of 925 individuals from the Ning1 × 7 F_2 *B. napus* population. The order of the individual lines from the population is arranged according to the increasing magnitude of the BcNEP2-induced ROS production.
(a) Histogram and density plot of flg22-induced ROS production of the F_2 population.
(b) Histogram and density plot of BcNEP2-induced ROS production of the F_2 population.
(c) ROS production in response to 20 nM of flg22.
(d) ROS production in response to 50 nM of BcNEP2. Data represent total RLU read over 40 min.

Assessment of phenotypic variation segregating with alleles for the highest marker at the A04 peak, Cab026058.1.2050.T, revealed that all accessions inheriting a 'G' at this locus (11 accessions) could respond to BcNEP2, and all accessions inheriting a 'T' (174 accessions) could not (Figure 1e; Table S2). For the highest marker at the C05 peak, Bo5g145300.1.259.T, 10 out of 17 accessions inheriting a 'T' at this locus could respond to BcNEP2, and 164 out of 165 accessions inheriting a 'C' could not (Figure 1e).

We calculated the LD with Cab026058.1.2050.T (A04) and found a region of 1.57 mb (Figure 1d) containing 250 genes in the *B. napus* pantranscriptome (Table S3). We calculated 1.48 mb in LD with Bo5g145300.1.259.T (C05) (Figure 1d), which corresponded to 252 genes in the *B. napus* pantranscriptome (Table S4). We performed BLASTP analysis to determine the putative *A. thaliana* orthologs of the *B. napus* genes in these two regions and found that these associations were not in homeologous genomic regions.

In addition to the major peaks, when the data obtained from NLP-responsive lines were processed in a quantitative manner rather than as binary values, we also noted a cluster of genes on A01 weakly but not significantly associated with NLP response (Figure S1).

BSA confirms a single dominant gene locus for NLP responsiveness on A04

To complement the AT analysis, we used BSA to establish whether both the A04 and C05 loci were responsible for NLP responsiveness. We developed a mapping population between Ningyou1 (NLP-responsive) and Ningyou7 (NLP-non-responsive), henceforth known as Ning1 × 7. All

Table 1 The phenotypical features of the selected individuals from F_2 population for the DNA pools

Phenotype	Pool1	Pool2	Pool3	Pool4
Magnitude of flg22-induced ROS	Low	High	Low	High
BcNEP2 responsiveness (−/+)	−	−	+	+
Magnitude of BcNEP2-induced ROS	−	−	Low	High

Individual F_2 plants were selected based on their magnitude of BcNEP2- and flg22-induced ROS production and their ability to recognise BcNEP2 molecule. 'Low' MAMP-induced ROS production defines individuals with ROS production lower than 1.0E5 RLU. 'High' MAMP-induced ROS production defines individuals with ROS production higher than 8.0E5 RLU. Classification of the individual plants according to their ability to recognise BcNEP2 molecule is defined as '−' for blind individual plants and '+' for the responsive.

F_1 plants from the Ning1 × 7 cross were heterozygous and responsive to BcNEP2 (Figures S2 and S3).

F_1 plants were selfed and F_2 seeds were obtained. ROS production by 50 nM BcNEP2 in responding F_2 individual plants ranged from $\sim 2.6 \times 10^3$ to 1.3×10^6 RLU (Figure 2a). One hundred and seventy-eight out of 925 F_2 individuals produced no ROS response following BcNEP2 treatment, representing ~19% of the population. This ratio was expected to be ~25% (3:1, responder: non-responder) if a single dominant gene model (X^2-test; $P < 0.001$) is predicted. Although the ratio obtained is close to that model, the slight difference between predicted and observed values could result from seedling selection during the transplanting process; some non-responding individuals were smaller and chlorotic and could have been selected against for vigour during transplantation. Since all heterozygote F_1 individuals are derived from at least one NLP-responsive parent, our combined results indicate a single dominant gene locus is responsible for NLP-responsiveness. All individuals from the cross could mount a ROS response to 20 nM flg22 to some extent, confirming that the cellular mechanisms for PTI were functional in NLP non-responders (Figure 2c).

Being responsive to BcNEP2 is a binary (yes/no phenotype) (Figure 2d), enabling the selection of 'Responsive' and 'Non-responsive' pools. Also, for those lines that do respond, the level of NLP-induced ROS has a normal distribution (Figure 2b), enabling creation of BSA pools for 'High responders' and 'Low responders' potentially enabling the identification of genes modulating the NLP response.

DNA pools for BSA were generated with individual F_2 plants selected from 5% of the extreme parts of the segregating population based on the binomial response to NLP (on/off), the magnitude of NLP response, and the magnitude of flg22 response (Table 1). Based on the calculation of 5% of the 747 NLP-Responsive F_2 plants, 30 individual F_2 plants were sampled per pool with response to 50 nM BcNEP2 and 20 nM flg22 ROS production (Table S5, Figure S4). Around ~1.8 billion raw sequence reads were obtained from each pool with a GC content of around ~38% in all samples, similar to the previously reported 40% for the *B. napus* ZS11 genome (Song et al., 2020).

The reads were aligned to the *B. napus* cv Darmor-*bzh* reference genome (Chalhoub et al., 2014) and genotypes of parental lines and the F_2 pools were investigated for the AT markers. Cab026058.1.2050.T on A04, inherited a 'C' rather than 'A' in NLP-responsive parent (Ningyou1) and the responsive pools when compared to non-responsive ones. A similar pattern was observed with the marker Bo5g145300.1.259.T on C05 with the parental lines possessing opposite genotypes, however random segregation of 'A' and 'G' genotypes was observed for all four F_2 pools (Figure S5).

To increase the coverage of the variations (SNPs and Indels) highly associated with the responsiveness to NLP, 'Responsive' (Pool3 and Pool4) and 'Non-responsive' (Pool1 and Pool2) pools were merged *in silico*. Of the 4 788 639 variations found, 3 713 757 could be anchored to Darmor-*bzh* chromosomes. After excluding variants identical between the parental lines and those with coverage <20, and quality under 2000, the total number of variants anchored to chromosomes decreased to 557 343. Each variant was scored with its corresponding bulk frequency ratio (BFR) value (Trick et al., 2012).

The variants with the highest BFR are located on A04 (Figure 3a), supporting the results from the AT (Figure 1). Variants with BFR value of infinity were also identified showing presence/absence polymorphisms between bulks. After applying the filters described above, the number of variants on A04 was detected as 24 660. On A04, 4 main peaks were obtained, the genomic length of the 1st and the 3rd peak was ~1 Mbp, the genomic length of the 4th peak was ~200 kbp and the genomic area covered by the highest peak (2nd) was spread on ~3 Mbp.

Additional minor peaks associated with NLP responsiveness were obtained on chromosomes A09, C01 and C04 (Figure 3a). Functional annotation and Arabidopsis homologues of the genes found within these regions are shown in Table S6. Effect predictions and functional annotations of the peak on C04 chromosome identified a putative RLP homologue *BnaC04g42570D*. However, it has been previously shown that from six species within the Brassica clade, only the species containing A or B genome can recognise NLPs (Schoonbeek et al., 2022). Therefore, the focus for further work was to define the candidate receptor gene on chromosome A04.

To delimit the region associated with the NLP responsiveness, we constructed a genetic map using KASP markers (Table S7) designed from highly associated SNPs identified in the BSA analysis. The computed BFR AO value (Bulk Frequency Ratio from alternative allele) and the

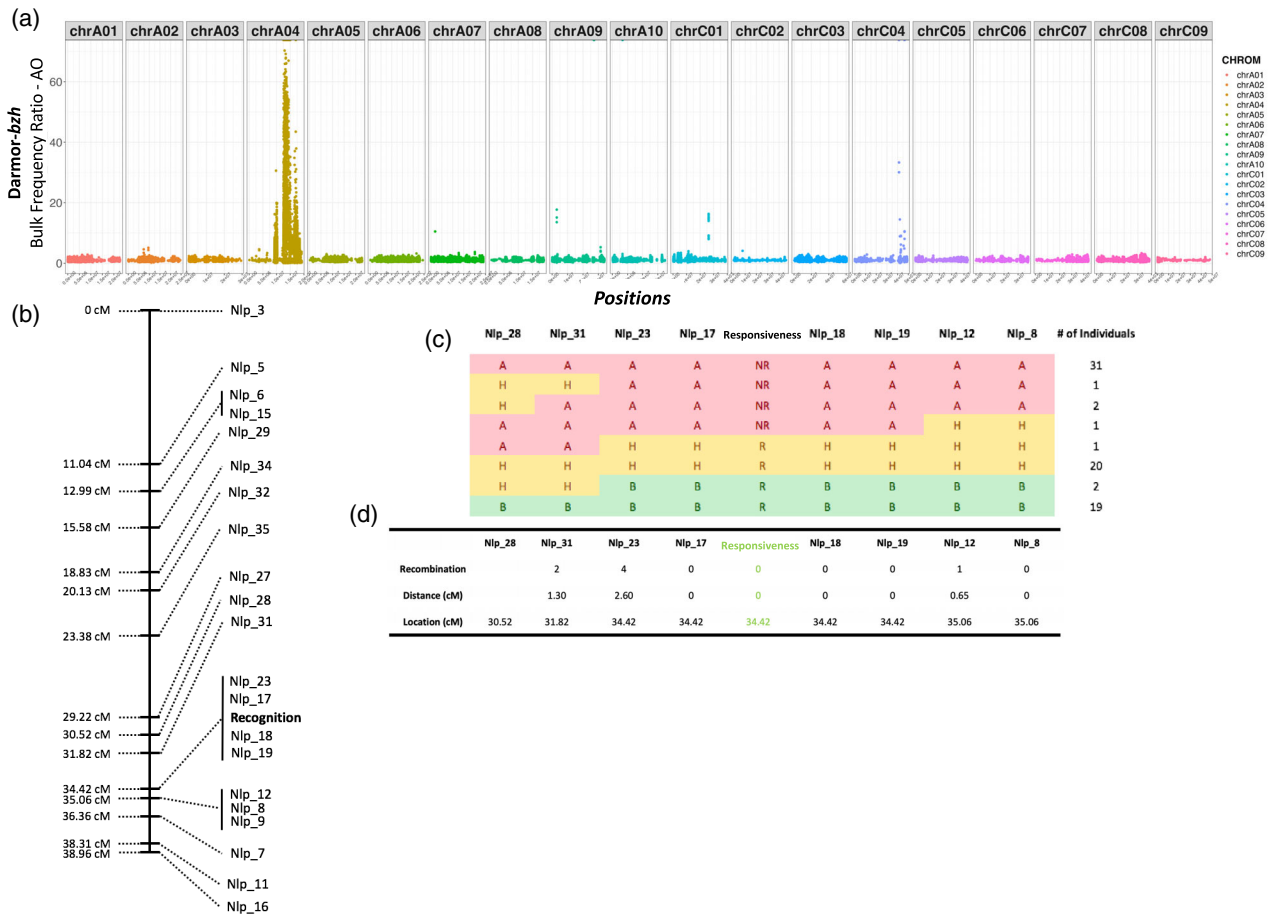

Figure 3. Genetic map of the NLP responsive region of the Darmor-*bzh* genome highly associated with 'BcNEP2-responsiveness'.
(a) Manhattan plot of the Bulk Frequency Ratios of variants called through *in-silico* merged 'Responsive' and 'Non-responsive' pools. After excluding the variants with lower than 20 read depth, 2000 quality and the same between parents, the positions of the 557 343 variants are plotted along *x*-axis on full genome.
(b) QTL map of 'BcNEP2-responsiveness' region of 77 plants from F_2 plants with 21 KASP markers.
(c) Genotypic features of each individual in the testing panel (in total 77 plants) for 8 KASP markers that are closely linked to BcNEP2-responsiveness [NR; Non-responsive (Red), R; Responsive (Green), H; Heterozygous (Yellow)].
(d) Details of each marker; number of recombinations between the adjacent markers and their corresponding locations on the generated genetic map.

functional predicted effects on the annotated genes of the SNPs (Table S8) were used as criteria for deciding the candidate SNPs to design KASP markers.

A DNA test panel with samples from 77 F_2 plants and parental lines was used to validate the 41 markers with specific FAM tail and HEX tail. Twenty-one out of 41 markers were suitable for genetic map construction ($P < 1.0E^{-10}$). Also, 9 out of 21 KASP markers were able to validate the responsiveness in the six other lines from the F_2 BSA population (Figure 3b). A quantitative trait locus (QTL) was mapped on A04, and SNPs highly associated with NLP response were delimited to 3.25 cM. Flanking markers NLP_31 and NLP_12 were 2.6 cM and 0.65 cM away from the markers linked to the locus of interest respectively (Figure 3c). Four markers (NLP_23, 17, 18 and 19) co-segregated with NLP responsiveness (Figure 3d).

The region associated with NLP responsiveness contains 23 RLP homologues that are not annotated on ZS11 genome

For the most significant peak on A04, 245 annotated genes were associated between marker BnDar.A04.12522928.C and BnDar.A04.17468291.C (Table S9). Among genes highly associated with the trait, homologues of Arabidopsis RLPs and those with LRR-type domain features were filtered and listed in Table S10. Although Darmor-*bzh* is the most improved and well-studied reference genome, it is non-responsive to NLPs (Schoonbeek et al., 2022), and therefore genes responsible for NLP responsiveness are likely to be absent or non-functional. In our analysis, we also used the genome sequence for Zhongshuang II (ZS11) (Song et al., 2020) which is NLP-responsive (Table S1). However, ZS11 is less well-annotated than Darmor-*bzh*.

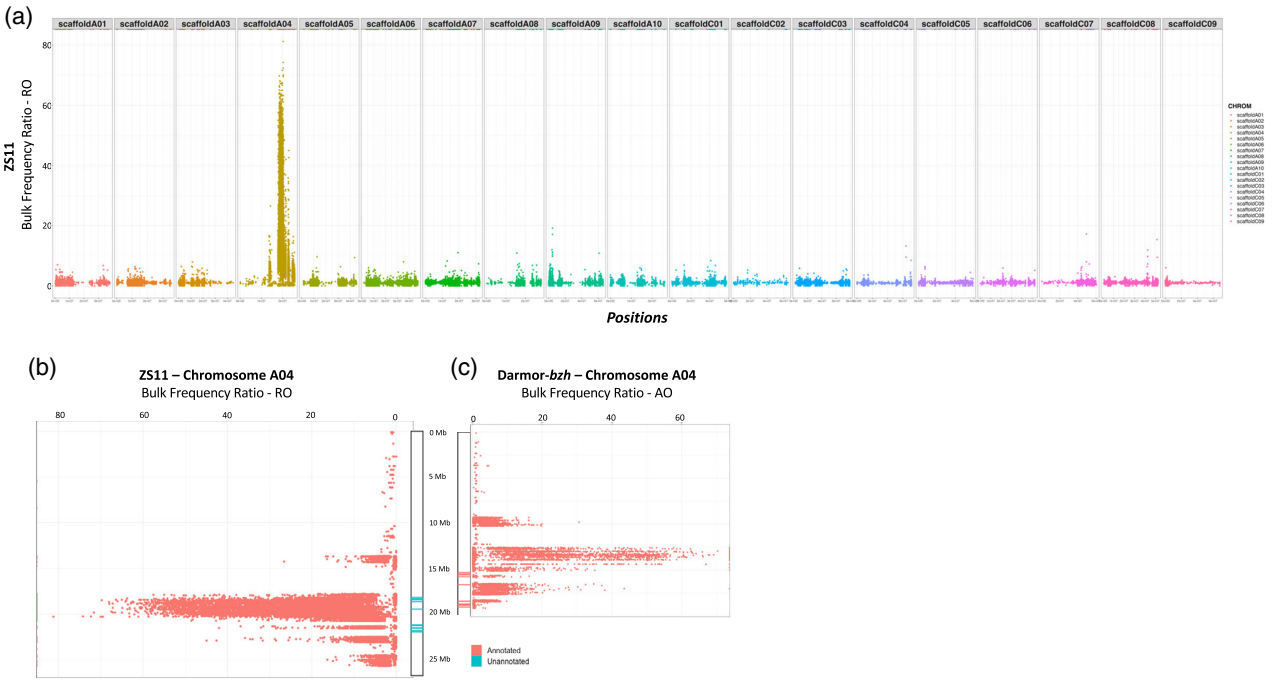

Figure 4. Manhattan plots of the Bulk Frequency Ratios of the variants called through *in-silico* merged 'Responsive' and 'Non-responsive' pools on the ZS11 genome.
(a) After excluding the variants with lower than 25 read depth, 1500 quality and the same between parents, the positions of the 801 366 variants are plotted along *x*-axis on the ZS11 genome.
(b) The positions of the 37 362 variants plotted along the *x*-axis on ZS11 A04 and (c) The positions of the 24 660 variants are plotted along the *x*-axis on Darmor-*bzh* A04. Regions containing homologues of *AtRLPs* which are annotated to a *Bna* gene in Darmor-*bzh* are illustrated in 'Orange', related regions present in ZS11 but not annotated to any *BnaZS* gene are illustrated in 'Blue'.

To further reduce the region associated with NLP responsiveness and to find possible candidate NLP receptor genes, the genomic data from bulks were aligned to the ZS11 reference. The BSA pipeline was performed and in total 3 672 282 variants were found anchored to ZS11 chromosomes. To exclude the false positives from the analysis, the thresholds were set at 1500 for quality and 25 for depth for the variants. After filtering steps, the total number of variants was 801 366 (Figure 4a) and, of those, 37 362 variants were anchored to chromosome A04. As expected, the highest peak was identified on A04, suggesting a strong association with the trait (Figure 4b). Between marker Bn.ZS.A04.17867537.C and Bn.ZS.A04.22885838.In total 391 annotated genes were found to be associated with the trait (Table S11).

The peaks identified on ZS11 A04 are more defined and have higher BFR values when compared with the results obtained with Darmor-*bzh* (Figure 4b,c). However, there were no annotated RLP homologues in the associated region on ZS11 genome (Table S12). The presence of genes annotated on A04 in Darmor-*bzh* was determined in the ZS11 genome using BLAST. The 23 RLP homologue genes within the associated region were also detected on the ZS11 genome with more than 80% identity (Table 2). ZS11 RNA-Seq data was then used to determine unannotated genes across the associated region. One potential candidate gene could be defined based on the presence/absence difference between the genomic data from the bulks and the parental lines. The un-annotated expressed putative gene located on ZS11 chromosome A04:20675496-20 678 125 was present in the NLP-responsive parent (Ningyou1) and absent in the non-responsive parent (Ningyou7) (Figure S6). This candidate region is located in the intronic region of *BnaA04G0210300ZS*. This gene shows annotation abnormalities, as the length of the gene in total is 23.7 kbp (found between position 20 673 147 and 20 696 865) and includes two exons, one of 190 bp and a second of 90 bp. Moreover, three further unannotated RLP homologues were located in the intronic region (Figure S6). Alignment of RNA-Seq data revealed that 10 out of 23 unannotated RLP homologues within the associated region are expressed, supporting the presence of these unannotated putative genes (Table 2).

BcNEP2-responsiveness enhances resistance to *B. cinerea* in *B. napus*

The effect of BcNEP2-responsiveness on *B. cinerea* disease resistance in *B. napus* was investigated using the segregating population (Figure 5a,b). There was a significant

Table 2 BLAST hits of the Darmor-bzh RLP homologue genes retrieved from A04 (between 9Mbp and 18Mbp positions) against ZS11 chromosome A04. Arabidopsis gene names and gene symbols of the RLP homologues are shared in 3rd and the 4th column.

Darmor-*bzh* Gene	Darmor-*bzh* Position	*A. thaliana* Gene ID	*A. thaliana* Gene symbols	ZS11 Gene	ZS11 Position	ZS11 Identity	Putative expression in ZS11
A04p19230.1_BnaDAR	14 616 835	AT1G74180.1	AtRLP14, RLP14; receptor-like protein 14	BnaA04T0165400ZS	17 449 828	100.00	
A04p19510.1_BnaDAR	14 758 027	AT3G25020.1	AtRLP42, RLP42; receptor-like protein 42		17 583 812	99.38	
A04p19700.1_BnaDAR	14 864 782	AT1G74180.1	AtRLP14, RLP14; receptor-like protein 14	BnaA04T0168900ZS	17 701 471	98.13	✓
A04p20070.1_BnaDAR	15 059 799	AT3G05650.1	AtRLP32, RLP32; receptor-like protein 32		17 905 249	99.13	✓
A04p21470.1_BnaDAR	15 892 698	AT5G40170.1	AtRLP54, RLP54; receptor-like protein 54	BnaA04T0182900ZS	18 680 607	98.16	✓
A04p24480.1_BnaDAR	17 607 762	AT2G32680.1	AtRLP23, RLP23; receptor-like protein 23		20 367 185	98.93	✓
A04p25180.1_BnaDAR	17 960 839	AT2G33020.1	AtRLP24, RLP24; receptor-like protein 24		20 368 719	87.30	✓
A04p25220.1_BnaDAR	18 005 314	AT3G24900.1	AtRLP39, RLP39; receptor-like protein 39		20 374 745	85.19	
A04p25150.1_BnaDAR	17 986 747	AT2G32680.1	AtRLP23, RLP23; receptor-like protein 23		20 374 802	86.20	
A04p25210.1_BnaDAR	17 998 645	AT2G32680.1	AtRLP23, RLP23; receptor-like protein 23		20 374 802	86.06	
A04p25110.1_BnaDAR	17 947 577	AT2G32680.1	AtRLP23, RLP23; receptor-like protein 23		20 375 084	86.87	
A04p24500.1_BnaDAR	17 616 444	AT2G32680.1	AtRLP23, RLP23; receptor-like protein 23		20 375 186	99.17	
A04p25200.1_BnaDAR	17 994 594	AT2G33020.1	AtRLP24, RLP24; receptor-like protein 24		20 383 895	85.23	✓
A04p25190.1_BnaDAR	17 986 178	AT2G33080.1	AtRLP28, RLP28; receptor-like protein 28		20 390 558	81.61	
A04p25020.1_BnaDAR	17 889 905	AT2G32680.1	AtRLP23, RLP23; receptor-like protein 23		20 642 171	100.00	
A04p25060.1_BnaDAR	17 912 709	AT2G32660.1	AtRLP22, RLP22; receptor-like protein 22		20 661 269	97.71	✓
A04p25070.1_BnaDAR	17 918 832	AT2G32660.1	AtRLP22, RLP22; receptor-like protein 22		20 668 658	96.78	
A04p25090.1_BnaDAR	17 928 707	AT2G33020.1	AtRLP24, RLP24; receptor-like protein 24	BnaA04T0210300ZS	20 678 150	95.67	
A04p25160.1_BnaDAR	17 974 891	AT2G32680.1	AtRLP23, RLP23; receptor-like protein 23	BnaA04T0210300ZS	20 682 276	94.45	✓
A04p25130.1_BnaDAR	17 955 802	AT2G33020.1	AtRLP24, RLP24; receptor-like protein 24	BnaA04T0210300ZS	20 683 256	96.86	
A04p25170.1_BnaDAR	17 976 340	AT2G33060.1	AtRLP27, RLP27; receptor-like protein 27	BnaA04T0210300ZS	20 683 739	93.98	
A04p25610.1_BnaDAR	18 210 000	AT2G33060.1	AtRLP27, RLP27; receptor-like protein 27		20 955 200	97.84	✓
A04p25140.1_BnaDAR	17 961 920	AT2G33020.1	AtRLP24, RLP24; receptor-like protein 24		21 089 544	83.52	✓

increase ($P = 4.262e\text{-}07^{***}$) in resistance to *B. cinerea* in BcNEP2-responsive lines (Figure 5c–g).

Botrytis cinerea lesion sizes of 60 individual plants, classified as low and high responders to each MAMP, flg22 and BcNEP2, were compared. There was no significant difference between 'low' and 'high' responders of BcNEP2 and flg22 for *B. cinerea* disease resistance. ($P\text{-value}_{flg22} = 0.597$, $P\text{-value}_{BcNEP2} = 0.439$) (Figure S7a,b). Overall, resistance of *B. napus* to *B. cinerea* infection is significantly affected by the ability to respond to BcNEP2, but not by the magnitude of either BcNEP2 or flg22-induced ROS response.

Brassica napus plants non-responsive to BcNEP2 have significantly higher flg22-induced ROS production

Interestingly, the ability of the plant to respond to BcNEP2 affects the magnitude of the response to flg22. There was

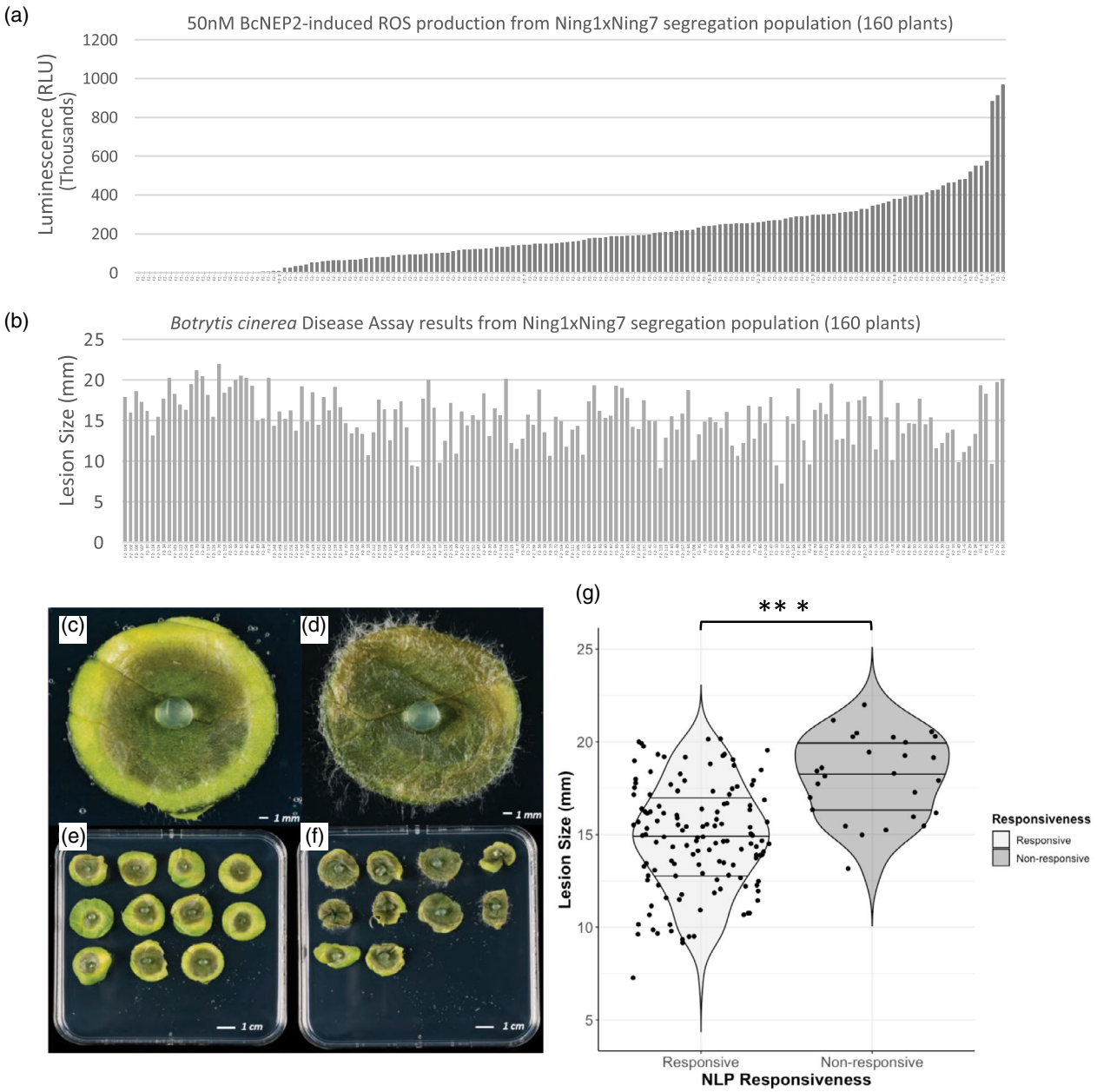

Figure 5. Phenotypic data of each of 160 individuals from Ning1 × 7 F_2 population from BcNEP2-induced ROS production and *Botrytis cinerea* disease assay. The order of the individual lines from the population is arranged according to the increasing magnitude of the BcNEP2-induced ROS production in the graphs.
(a) ROS production in response to 50 nM of BcNEP2. Data represent total RLU read over 40 min.
(b) Lesion sizes of *B. cinerea* infection. Data represented as lesions size (mm) of *B. cinerea* infection on *B. napus* plant leaves 3 dpi.
(c) *B. cinerea* infected leaf disc taken from a 'Responsive' F_2 plant.
(d) *B. cinerea* infected leaf disc taken from Ningyou7 (Non-responsive to NLP) which is the parental line of the F_2 population.
(e) A plate overview containing leaf disc samples from the 'Responsive' F_2 plant.
(f) A plate overview containing leaf disc samples from the 'Non-responsive' F_2 plant. Five-week-old *B. napus* leaf discs were infected with *B. cinerea* plugs. Leaves were photographed at 3 dpi.
(g) Violin plot illustrating the distributions of lesion sizes belongs to 2 different groups of 133 Responsive (light grey) and 27 Non-responsive (dark grey) F_2 individuals, showing the significant differences between the groups (*P*-value = 4.262e-07***).

a significant difference between the BcNEP2-responsive and non-responsive F_2 plants in their flg22-induced ROS response with the mean ± SEM value as 82 985 ± 5700 RLU and 135 349 ± 20 872 RLU, respectively (*P*-value = 0.00247 **) (Figure 6). When only the BcNEP2-responsive F_2 plants were used in the correlation analysis, there was a

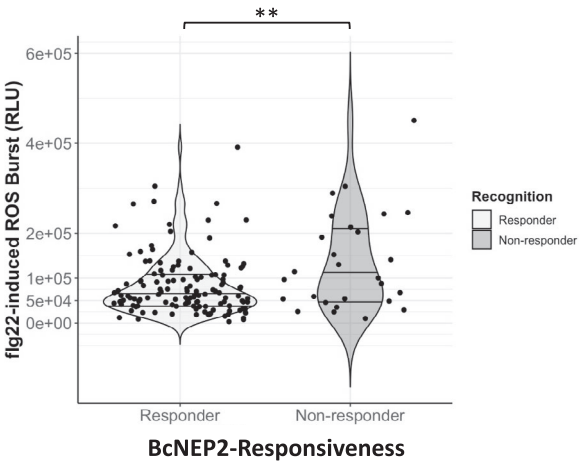

Figure 6. BcNEP2-responsiveness affects the magnitude of flg22-induced ROS production. (a) Violin plot illustrating the distributions of flg22-induced ROS production belongs to 2 different groups of 133 Responder (light grey) and 27 Non-responder (dark grey) F_2 plants, showing the significant differences between the groups ($P = 0.00247$ **).

significant positive correlation between the magnitude of ROS production in response to BcNEP2 and flg22 with a correlation coefficient of 0.58 (Figure S8).

BSK1 is associated with modulating the NLP response

Genomic data from Pool4 (High BcNEP2-responsive) and Pool3 (Low BcNEP2-responsive) were run in the BSA pipeline to identify genes potentially modulating the magnitude of the BcNEP2-induced ROS production. In this study, 3 769 915 variants were anchored to chromosomal positions on the ZS11 genome of which, after filtering, 2 753 844 variants remained with more than 1500 quality score and 25 depth (Figure S9a).

A peak on A01 associated with high BcNEP2-responsiveness was spread on ~7.7 Mbp between 1.6 and 9.3 Mbp (Figure S10). In that region, 418 annotated genes were found to be likely affected by variants, with the lowest BFR value of 4. From those, 328 genes were identified to have homologues in Arabidopsis (Table S15). Annotation and effect prediction of 131 variants on A01 were associated with the high BcNEP2-responsiveness phenotype, including *BnaA01G0031400ZS* (Table S16), a homologue of *Arabidopsis BR-SIGNALLING KINASE1* (*AtBSK1; At4g35230*), which is physically associated with FLS2 in Arabidopsis (Shi et al., 2013). The *BnaBSK1* orthologue on A01 (Figure S11) was also included in the list of genes weakly but not significantly associated with NLP response within the AT analysis (Figure S1).

To detect the variants associated with high flg22-responsiveness, the same protocol was followed with Pool1 (Low flg22-responsive) and Pool2 (High flg22-responsive) (Figure S9b). The most defined peak was on A02 spreading on ~450 kbp, between position 1.5 and 1.95 Mbp (Table S13). In that region, 64 annotated genes were likely affected with the highest BFR value of 18 (Table S14).

Since BSK1 has previously been shown to be a co-receptor with FLS2 for flg22-mediated PTI, we hypothesised that it may have a similar role in NLP-mediated response. To functionally test this Arabidopsis *bsk1-1* mutants were compared with Col-0 following genotyping to confirm the mutations (Figure S12). ROS production of *bsk1-1* and Col-0 was compared using different concentrations of BcNEP2 and flg22. There was a gradual decrease in ROS production corresponding to decreasing concentration of both MAMPs. Similar results were observed in Col-0 by both BcNEP2 and flg22 MAMP motives. In contrast to the results of Shi et al. (2013), there was no significant difference between the wild type and *bsk1-1* mutant line for any concentration of flg22 (Figure S13). However, unlike the flg22 response, a significant difference was found between the *bsk1-1* mutant and the Col-0 in response to 50 nM BcNEP2 (Figure 7a,b). This significant difference shows that *BSK1* is involved in BcNEP2-triggered ROS production in Arabidopsis. The *bsk1-1* mutant line was significantly more susceptible to *B. cinerea* wild-type strain with larger lesions compared to Col-0 (Figure 7c,d).

DISCUSSION

The most likely receptor candidates are expected to be RLP-like genes since these are required for perception of the NLPs to initiate the signalling mechanism (Albert et al., 2015). With BSA using the well-annotated Darmor-*bzh*, we defined a clear peak associated with NLP responsiveness covering a ~3 Mbp region on A04. The region was delimited to a maximum of 3.25 cM which could be covered with 21 KASP markers, four of which were co-segregating with NLP-responsiveness. Using the combined Darmor-*bzh* and ZS11 genomes and transcriptomic data for ZS11, we identified 23 RLP homologues within the region, ten of which were expressed (Table 2). However, we could not define with confidence a specific RLP homologue responsible for NLP responsiveness. In future studies to confirm the candidate gene, the complexity of RLP genes in this region of the polyploid *B. napus* genome should also be taken into account as it may contribute to quantitative variation in NLP response by affecting transcription and protein abundance. Future research to evaluate specific or multiple RLP homologues and their respective contribution to total NLP responsiveness could be undertaken using CRISPR-Cas-9-mediated editing of an NLP-responsive *B. napus* accession such as ZS11.

Our results demonstrate that NLP responsiveness is associated with enhanced resistance to *B. cinerea* in *B. napus* confirming a previous report of RLP23-mediated resistance in Arabidopsis (Ono et al., 2020). However, this

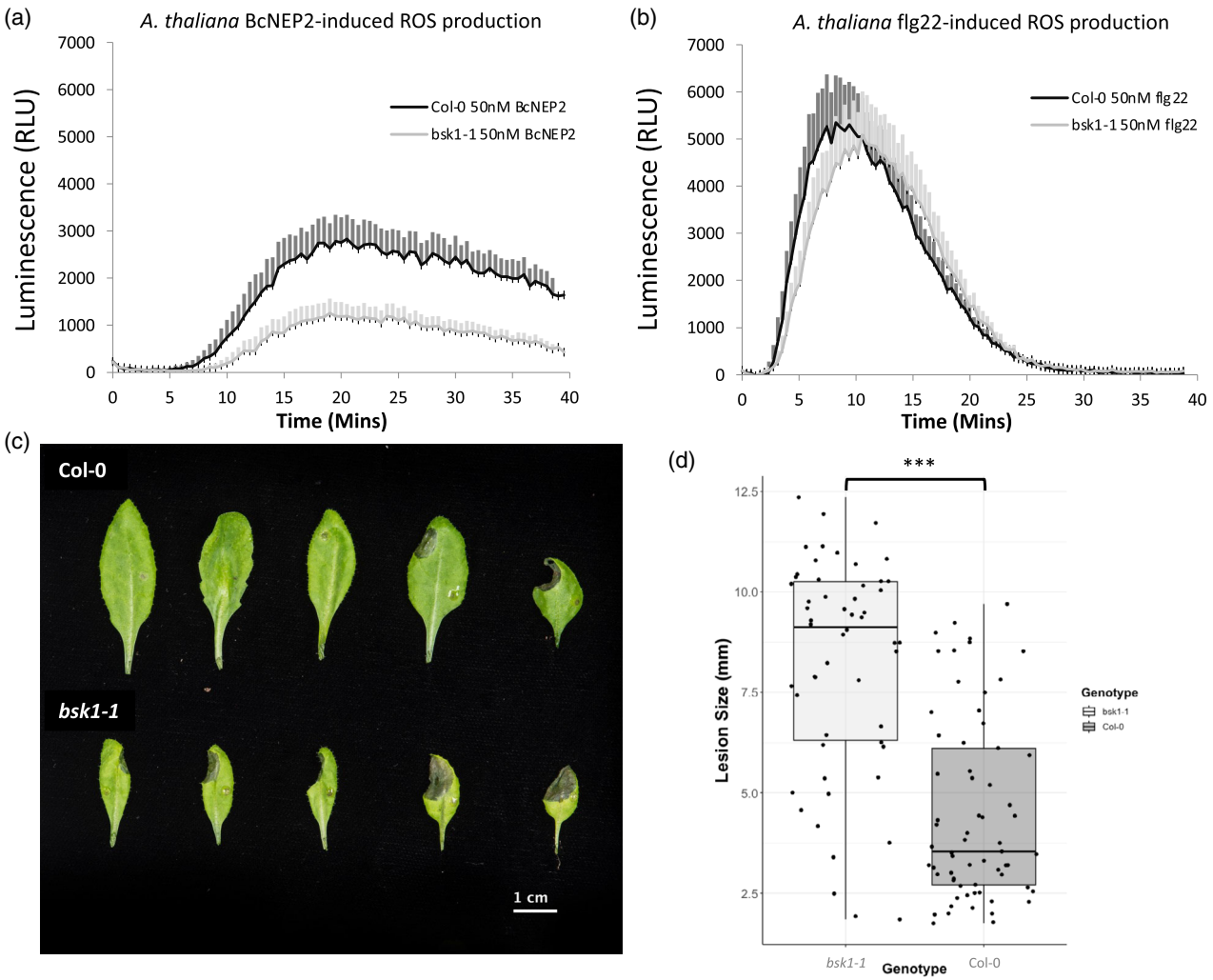

Figure 7. BSK1 is involved in BcNEP2-induced ROS production and *B. cinera* disease resistance. Leaves of the Col0 (wild type), *bsk1-1* mutant lines were treated with (a) 50 nM BcNEP2 and (b) 50 nM flg22 incubated with luminol and horseradish peroxidase to detect ROS. Data represent RLU read over 40 min. Error bars are the standard error of eight biological replicates (*P*-value = 0.0287*). *Botrytis cinerea* disease screening of leaves from Arabidopsis plants. (c) Five-week-old Arabidopsis plants were infected with *B. cinerea*. Five microlitres of drops from B05.10 strain placed on the upper part of the leaf. The plants were photographed at 3 dpi. (d) Box plot representing lesion size of *B. cinerea* infection on Arabidopsis plant leaves 3 dpi. Each dot represents lesion sizes from 12 biological replicates (*P*-value = 1.12E-14***).

contrasts with the previous study in *B. napus* where no association was observed (Schoonbeek et al., 2022). In that study, two responsive *B. napus* cultivars (N02D, Ningyou1) were compared with non-responder cultivars (Tapidor, Ningyou7) and no difference in resistance against *B. cinerea* was observed (Schoonbeek et al., 2022). However, the cultivars used had different genetic backgrounds and so other genes could mask the effect of NLP-triggered immunity against *B. cinerea* disease resistance in *B. napus*. The considerable amount of genetic similarity between Ningyou1 and Ningyou7 parental lines (Wang et al., 2017; Zou et al., 2019) was effective at eliminating background genetic variation which might interfere with the disease assay results.

Comparison of 'high' and 'low' responders enabled the identification of candidate genes involved in modulating the response to NLPs. Of these genes, we hypothesised that BSK1 might be a candidate since it has previously been shown to be a co-receptor in the flg22-mediated response in Arabidopsis (Shi et al., 2013). Our preliminary results suggest this may be the case, since BcNEP2-induced ROS production was significantly reduced in Arabidopsis *bsk1-1* mutant lines. However, there was no reduction in flg22-mediated ROS burst as previously reported (Shi et al., 2013). We suggest that *BSK1* may be involved in NLP response possibly through its involvement in a complex similar to that reported for BAK1/SOBIR1 (Albert et al., 2015). As expected from previous research

(Ono et al., 2020), the relative *B. cinerea* lesion size was enhanced in the *bsk1-1* mutant lines. However, it was noted that the leaf size of *bsk1-1* mutant plants was reduced compared to Col-0. Our results provide a preliminary indication of the involvement of BSK1 in NLP-mediated response during PTI.

When compared to BcNEP2-responsive plants, the BcNEP2-non-responsive group had a significant increase in the amount of flg22-induced ROS (Figure 6a). In Arabidopsis, the downstream immunity-related genes upregulated by NLPs strongly overlapped with the genes that are induced by flg22 (Oome et al., 2014; Oome & Van den Ackerveken, 2014; Wan et al., 2019) and the downstream components of signalling cascades are shared between the different PRRs (Albert et al., 2015). Thus, competition for the shared common co-receptors for different PRRs may operate during signal transduction, explaining the increased capacity to respond to the flg22 molecule in the absence of the NLP receptor.

Overall, our study combines a series of investigations into the perception of NLPs in *B. napus* and how it contributes to disease resistance. We show that NLP responsiveness induces disease resistance in *B. napus*, define a complex RLP locus associated with this and demonstrate the potential involvement of BSK1 in modulating the response. Overall, our results demonstrate the challenges and opportunities of translational research to transfer knowledge from model organisms to complex polyploid crop species.

EXPERIMENTAL PROCEDURES

Plant material

A *B. napus* diversity panel of 189 lines from the Renewable Industrial Products from Rapeseed (RIPR) panel was used for AT analysis (Havlickova et al., 2018). Genotypes were split into four batches for sampling and two experimental replicates were performed.

For BSA analysis, reciprocal crosses between semi-winter oilseed rape (OSR) accessions Ningyou1 and Ningyou7 (Source, OCRI, Wuhan, China) were generated by manual crossing with two replicates. Tapidor, a winter OSR accession, from the *B. napus* diversity set and Brassica Germplasm Collection at the John Innes Centre, UK, was used as a control accession. Parental lines for crossing and F_1 plants for seed production were sown in Levington F2 with grit and grown in a glasshouse with a 16-h photoperiod at 18/12°C Day/night temperatures (~6 months). For disease and MAMP assays, plants were grown in Levington F2 with grit for 4–5 weeks in controlled environment rooms (CERs) at 22°C, 70% relative humidity, under 10/14 h day/night cycle.

Arabidopsis plants were sown in Levington F2 with 15% 4 mm grit in 24-cell trays. Seeds were stratified in the dark for 2 days at 4–5°C and trays were covered with a transparent plastic lid for the first 1–2 weeks. Plants were grown at 20–22/18–20°C Day/night, 70% relative humidity, under 10/14 h day/night cycle in a CER for 5–6 weeks prior to phenotyping. Arabidopsis *Atbsk1-1* mutant seeds and Col-0, used as wild type, were obtained from Prof. Dingzhong Tang, Chinese Academy of Sciences (Nie et al., 2011).

Reactive oxygen species (ROS) assay

Microbe-associated molecular pattern (MAMP) peptides

Peptides of flg22 (22 amino acid long flagellin fragment; QRLSTGSRINSAKDDAAGLQIA, Peptron http://www.peptron.co.kr, Korea, dissolved in sterile H_2O at 10 mM) and BcNEP2 (*Botrytis cinerea* Necrosis and Ethylene-inducing protein 2; AIMYSWYMPK-DEPSTGIGHRHDWE, Genscript www.genscript.com, at 87.5% purity and dissolved in DMSO at 10 mM) were used for detection of oxidative burst.

Detection of oxidative burst

A luminol/peroxidase-based assay was used to measure MAMP-induced reactive oxygen species (ROS) production (Lloyd, 2014). Four millimetre of leaf discs from *B. napus* (3rd leaf) or Arabidopsis were incubated in 200 µl of sterile water in a 96-well plate overnight, in the dark, at room temperature. The water was replaced by 100 µl solution containing; 0.2 nM luminol at 34 mg L^{-1}, horseradish peroxidase (HRP) at 20 mg L^{-1} (Sigma-Aldrich Inc., St. Louis, MO, USA), and the selected MAMP at concentrations of 50 nM, 20 nM, 10 nM or 2 nM. Luminescence over a 40-min period was displayed as photon production quantitated as relative light units (RLUs). Emitted photons were counted using a Varioskan Flash plate reader (ThermoFisher Scientific, Waltham, MA, USA).

Botrytis cinerea disease assays

Botrytis cinerea strain B05.10 (Schoonbeek et al., 2001) was grown on 1/5 Potato Dextrose Agar (PDA) or on MEYAA plates including; Malt Extract Agar (MEYA, OXOID# CM0059) at 30 g L^{-1} with Yeast extract at 2 g L^{-1} and Agar (FORMEDIUM) at 5 g L^{-1} at 21°C. *B. cinerea* plates were grown for at least 2 weeks before collecting spores.

One day prior to the inoculation, 200 µl of *B. cinerea* spores with 2.5×10^6 spores ml^{-1} concentration were spread on 1/5 PDA plates and grown at 21°C. Leaf discs (22 mm, single disk/plant, up to 16 replicates) cut from the 4th leaf of *B. napus* plants were placed on 0.6% water agar plates in square Petri dishes in the dark, overnight. The next day, leaf discs were inoculated with *B. cinerea* plugs (4 mm diameter) and incubated in a CER at 21°C with a relative humidity of 85–100% with photon flux density of 10–20 µmol m^{-2} sec^{-1}. Lesion size was measured after 3 days with digital callipers.

Prior to inoculation, *B. cinerea* spores were diluted to 2.5×10^5 spores ml^{-1} in 1/2 Potato Dextrose Broth (PDB) solution and shaken at room temperature for 90 min. Five microlitres of droplets from the spore solution were placed on selected 5–6 leaves of individual Arabidopsis plants grown in 24-cell trays. Trays were covered with plastic lids, sealed with parafilm and transferred to a CER at 21°C with a relative humidity of 85–100% and low light (10–20 µmol m^{-2} sec^{-1}). Lesion sizes were measured after 3 days with digital callipers.

Associative Transcriptomics (AT)

Total RLU over 40 min was calculated using a linear fixed- and random effects model with *B. napus* genotype as a fixed effect and experimental replicate and batch as random effects. Estimated marginal means were calculated for each *B. napus* genotype using *emmeans* (version 1.8.0) (R package). These data were transformed into binary values (1 or 0, for responding and non-responding lines, respectively) for AT analysis.

The RIPR genotype (SNP) and expression level datasets (Havlickova et al., 2018) were obtained from York Knowledgebase (http://yorknowledgebase.info). This dataset was reduced to only include accessions used in this study. Our recently updated population structure (Fell et al., 2023) was used for the AT analysis.

Mapping was performed using an R-based pipeline (Nichols, 2022) using GAPIT Version 3 (Lipka et al., 2012; Wang & Zhang, 2021). Analyses were conducted using a generalised linear model (GLM); Bayesian-information and Linkage-disequilibrium Iteratively Nested Keyway (BLINK) (Huang et al., 2019), and Fixed and random model Circulating Probability Unification (FarmCPU) (Liu et al., 2016) to determine the optimal model. The false discovery rate (FDR) was determined using the Shiny implementation of the q-value R package (Storey, 2011).

To determine specific marker Linkage Disequilibrium (LD) we calculated the mean pairwise R^2 for the peak marker to all markers on the chromosome using TASSEL Version 5.0 using the site by all analysis option (Bradbury et al., 2007). Markers were considered in LD when $R^2 > 0.2$.

Bulk segregant analysis (BSA)

Creation of F_2 segregant population

Five seeds from each Ningyou1 and Ningyou7 F_1 cross were sown and leaf samples from each F_1 plant were used for DNA isolation with the DNeasy® Plant kit (Qiagen, Venlow, The Netherlands). Publicly available microsatellite markers (http://www.brassica.info/resource/markers/ssr-exchange.php) were used to detect polymorphic markers between the parental accessions. sR12095, (Table S17, Figure S2) was used to confirm F_1 crosses with a heterozygous genotype. PCR with SSR sR12095 (Agriculture and Agri-Food Canada AAFC) was conducted using AmpliTaq Gold™ DNA Polymerase (ThermoFisher Scientific) in a final reaction volume of 20 µl with 2 µl of the diluted genomic DNA (100 ng), 0.5 µM from each primer pairs, 2 µl PCR buffer, 1 unit AmpliTaq Gold™ DNA Polymerase (5 u μl^{-1}), 2.5 mM dNTPs and water to 20 µl. The PCR programme had a denaturation step at 94°C for 10 min followed by 8 cycles of 94°C for 15 sec, 50°C for 15 sec and 72°C for 30 sec followed by 32 cycles of 94°C for 15 sec, 50°C for 15 sec, 72°C for 30 sec and ending at 8°C. DNA bands were visualised on 3.0% Agarose gel using Alphalmager EP. Each plant was phenotyped for ROS production with 50 nM BcNEP2 and 20 nM flg22. Successfully crossed F_1 plants were selfed to develop the Ningyou1 × Ningyou7 (Ning1 × 7) F_2 population. 960 F_2 seeds were sown and grown under CER conditions as ROS phenotyping for BSA.

Experimental design – creation of bulked DNA pools

BcNEP2-induced ROS production data from the F_2 population was normally distributed (Figure 2). Extremes from the tails of the normal distribution representing ~5% of the population (30 of 747 NLP-responder lines) were selected to create DNA pools with the phenotypic features (Figure S4; Table 1).

To isolate DNA from the *B. napus* leaves for sequencing, leaf tissue from individual F_2 plants was collected and frozen at −80°C using liquid Nitrogen. In this study, 0.05 g leaf samples from each selected line were bulked for grinding to create pools. To ensure the same quantity of samples was used for each pool and the parental samples, 1.5 g of leaf material was used for parental lines. DNA was isolated using an improved CTAB-based method (Tudor et al., 2020).

Sequencing and Bulk Segregant Analysis

Illumina sequencing (350 bp insert DNA library, 150-bp paired-end reads, 40× coverage, via Illumina NovaSeq PE150 Platform) was performed for the bulked pools and parents. Sequence quality was evaluated with *FastQC* v0.11.8 (https://www.bioinformatics.babraham.ac.uk/projects/fastqc/). Reads were aligned to *B. napus* reference genomes Darmor-*bzh* (Chalhoub et al., 2014) and Zhongshuang11 (Song et al., 2020) using *bwa* v0.7.1 (Li & Durbin, 2010). The resulting SAM files were converted to BAM files using *samtools* v1.9 (Danecek et al., 2021). SNP calling was performed per chromosome using *freebayes* v1.1.0.46 (Garrison & Marth, 2012). To define the filtering thresholds and to exclude the false positive variations from the analysis, histogram plots were created using *ggplot2* package (Wickham, 2016) with the quality and the depth of the variations (Figure S14). Filtering was applied using *bcftools-1.8* (Danecek et al., 2011) to exclude variations with quality lower than 2000, depth lower than 20 and those coming from Darmor-*bzh*. Markers were named according to the reference genome ('BnDar' for Darmor-*bzh* and 'BnZS' for Zhongshuang11), chromosome/scaffold type (A or C) and number (01 to 10), genomic position on the related chromosome and sequence of the alternative variant.

For variations with an informative base derived from a responsive background, the Bulk Frequency Ratio (BFR) was calculated by dividing the frequency in the responsive bulk by the frequency in the non-responsive bulk (Trick et al., 2012). The formula for calculation of the BFR values for each variant is [Counts of Alternative (Alt) variation is called as AO, counts of Reference (Ref) variation is called RO and count of total reads (Depth) is called DP in the formula]:

$$R_{\text{index}} = \frac{\text{RO}}{\text{DP}}$$

$$A_{\text{index}} = \frac{\text{AO}}{\text{DP}}$$

$$\text{BFR}_{\text{responsive}} = \frac{R_{\text{index}}}{A_{\text{index}}}$$

$$\text{BFR}_{\text{non responsive}} = \frac{A_{\text{index}}}{R_{\text{index}}}$$

The *ggplot2* package (Wickham, 2016) was used to create the Manhattan plots with BFR values of each variant anchored to the chromosomes.

SnpEff was used to predict the effects of genetic variants on genes and proteins (Cingolani, Platts, et al., 2012). Related information from VCF files was obtained through *SnpSift* (Cingolani, Patel, et al., 2012). BioMart database (Durinck et al., 2005, 2009) was used to identify Arabidopsis homologues and coded domain features of the *B. napus* genes.

All the code used in BSA is available on the github repository: https://github.com/hicretyalcin/BSA_Brassica_napus.

KASP assay

Kompetitive allele-specific PCR (KASP) markers were developed by using PolyMarker (Ramirez-Gonzalez, Uauy, et al., 2015). A 200 bp genomic sequence, including the SNP, was generated to start the pipeline. The list of the SNPs used in KASP marker design, along with their corresponding features, is shown in Table S18. Designed primers included standard FAM or HEX compatible tails [FAM tail: 5′-GAAGGTGACCAAGTTCATGCT-3′; HEX tail: 5′-GAAGGTCGGAGTCAACGGATT-3′ (Sigma-Aldrich Inc.)] (Table S7). DNA was isolated from samples with known phenotypes from the F_2 population with DNeasy® Plant kit (Qiagen). The DNA plate contained 21 lines from: each bulked Pool (Pool1, Pool2, Pool3 and Pool4); 3 individual plant DNA samples from Ningyou1; 3 individual plant DNA samples from Ningyou7 and

DNA samples of 6 different NLP-responsive *B. napus* lines (Swu8, Yudal, Chuanyou2, Tribune, Taisetsu and ZS11) respectively.

For the KASP Assay, DNA was diluted to 10 ng μl^{-1}, then 1.8 µl of DNA was dispensed into 384 well PCR plate and dried in an incubator. PCR mastermix containing 1.2 µl water, 1.2 µl PACE® (3CR Bioscience, Harlow, Essex, UK) mix and 0.03 µl primer mix per well was dispensed to the wells. Primer mix was 46 µl water, 12 µl of each forward primer and 30 µl of the common reverse primer. The PCR programme was 94°C for 15 min followed by 10 touchdown cycles at 94°C for 20 sec and 65°C for 1 min, dropping by 0.8°C per cycle to 57°C. Then another 45 cycles at 94°C for 20 sec and at 57°C for 1 min. The plate was then read on a BMG PHERAstar plate reader and scored using LGC's *Klustercaller* program.

Genetic map construction

Linkage analysis was made by using R version 3.6.1 with the *qtl* package version 1.46-2 (Broman, 2003). Genetic distances of each marker to the phenotype based on recombination frequency was calculated.

Detection of expressed putative genes on ZS11 genome

RNA-Seq data from ZS11 obtained from the Brassica Rapeseed and Vegetable Optimisation (BRAVO) consortium was aligned to the genome sequence (Song et al., 2020) using hisat2 (Kim et al., 2019), version 2.1.0 with standard parameters. Resulting SAM files were sorted and converted to BAM format using samtools (Danecek et al., 2021), version 1.10. Regions of interest in the genome were manually inspected using Integrative Genomics Viewer (IGV) (Robinson et al., 2011). *A. thaliana* homologues were assigned by reciprocal BLAST search strategy. Gene IDs obtained as hits after performing BLAST search (*e*-value cut off 1e-5) against Darmor-*bzh* v10 using TAIR genome as query, were used as query genes to run a reciprocal blast search with TAIR genome as target (*e*-value cut off 1e-5). Genes were marked as mapped if the reciprocal blast query Darmor-*bzh* gene returned the same *A. thaliana* gene as the highest scoring hit with the original Darmor-*bzh* gene with an *e*-value <1e-5 in the previous search.

Genotyping of *A. thaliana bsk1-1* mutants

DNA from Arabidopsis leaf samples was extracted with DNeasy® Plant kit (Qiagen). All samples were verified to contain the *bsk1-1* mutation using PCR with cleaved amplified polymorphic sequence (CAPS) primers (Shi et al., 2013) (Table S17) followed by a digestion with BsuRI (HaeIII) and visualisation on 2.4% agarose gels.

AUTHOR CONTRIBUTIONS

All in vivo experiments were conducted by HAY with help from RK and EV who contributed to bulk sampling and phenotyping. RW and H-JS contributed to population development and experimental design. H-JS contributed to phenotypical data collection for AT analysis. HAY and RHRG performed all bioinformatics associated with the BSA, KASP marker design and mapping. CNJ performed AT analysis. BS and GSS performed all bioinformatical analyses associated with RNA-Seq data. HAY wrote the manuscript. CR and RW supervised and co-directed the research and edited the manuscript. All authors read and approved the final manuscript.

ACKNOWLEDGEMENT

HAY was supported by The Newton-Katip Celebi Fund given by the British Council and The Scientific and Technological Research Council of Turkey (TUBITAK). RHRG was supported by the UK Biotechnology and Biological Sciences Research Council (BBSRC) through the Designing Future Wheat (BB/P016855/1) Institute Strategic Program and the European Research Council (ERC-2019-COG-866328). CJR was supported by BBSRC grants BB/N005007/1 (MAQBAT) and the Plant Health Institute Strategic Programme BB/P012574/1 'Response' subprogramme BBS/E/J/000PR9796. HJS and RK were supported by BB/N005007/1. RW, CNJ and GSS acknowledge financial support from Institute Strategic Programme 'Genes in the environment' (BB/P013511/1) and BBSRC Brassica Rapeseed And Vegetable Optimisation strategic Longer and Larger fund (BRAVO sLOLA) (BB/P003095/1). We thank the BRAVO sLoLa research team for access to gene expression data. We are grateful to Dingzhong Tang (CAS) for providing Arabidopsis *bsk1-1* mutant seeds. The authors would like to thank Horticultural Services in JIC for their valuable support in growing plants.

CONFLICT OF INTEREST

The authors declare no conflict of interest.

DATA AVAILABILITY STATEMENT

All raw sequence reads from Ningyou1, Ningyou7 and the four DNA pools have been deposited in the European Nucleotide Archive (ENA) under PRJEB65877. For access to RNA-Seq data from ZS11 from the BRAVO consortium please contact brassica@jic.ac.uk.

SUPPORTING INFORMATION

Additional Supporting Information may be found in the online version of this article.

Figure S1. Manhattan plot showing marker-trait association for quantitative ROS production to BcNEP2 on A01. Black line indicates FDR <0.05 which is correspond to −log10(*P*) value of 6.64 while the value of *BnaBSK1* orthologue is found as 6.44.

Figure S2. Amplification of microsatellite marker sR12095 in reciprocal crosses and parental lines. The fragments were separated in a 3.0% denatured Agarose gel. To visualize the amplified PCR products, 6× loading dye was added to PCR products before loading onto an agarose gel containing ethidium bromide and 15 µl of PCR products were run on Agarose gel. The 1st, 12th and 15th lanes of are 100 bp DNA Ladder (NEB #B7025). The rest of the lanes and their corresponding sample names are represented in the figure. Polymorphism of microsatellites among the Ningyou1 (Ning1) and Ningyou7 (Ning7) parents seen on the last lanes on the right side of the gel.

Figure S3. PAMP-induced ROS production from 10 F1 plants derived from 2 different reciprocal crosses (a) 50 nM BcNEP2-induced ROS burst from 3rd leaves of Ningyou1 × Ningyou7 F1 plants. (b) 20 nM flg22-induced ROS burst from 3rd leaves of Ningyou1 × Ningyou7 F1 plants. Bars represent Total Relative Luminescence Unit (RLU) read over 40 min. Error bars are the standard error of 8 biological replicates.

Figure S4. The selection of the pools based on their corresponding: (a) 50 nM BcNEP2-induced ROS production (b) 20 nM flg22-induced ROS production. Highlighted regions on bar plots illustrating the distributions of ROS production belonging to 4 different DNA pools of 30 F2 individuals from BSA population; Pool1

(NLP-nonresponsive, low flg22 response), Pool2 (NLPnonresponsive, high flg22 response), Pool3 (low NLP response, low flg22 response), and Pool4 (High NLP response, High flg22 response), showing phenotypic differences between the pools.

Figure S5. Genotyping results of Ningyou1, Ningyou7 and F2 pools for AT markers on A04 and C05. Illustration generated from Integrative Genomics Viewer (IGV) captured the area of (a) "chrA04:13395345-13395385" and (b) "chrC05:41790450-41790489" on Darmor-*bzh* genome. From top to bottom, the panels are representing the aligned data of DNA-Seq data from Ningyou1, Ningyou7, Pool 1, Pool 2, Pool 3 and Pool 4. And the bottom panel representing the corresponded annotated genes; *BnaA04g16410D* on A04 and *BnaC05g46250D* on C05 respectively. Location marked with line is showing the genotype of parental lines and the F2 Pools for GWAS markers; Cab026058.1.2050.T and Bo5g145300.1.259.T.

Figure S6. Illustration generated from Integrative Genomics Viewer (IGV) captured the area of "scaffoldA04:20672218-20697330" on ZS11 genome. From top to bottom, the panels are representing the aligned data of (1) RNA-Seq data from ZS11, (2) DNA-Seq from Responsive parent (Ningyou1) (3) DNA-Seq from Non-responsive parent (Ningyou7). And the bottom panel representing the corresponded annotated gene *BnaA04G0210300ZS*. Region highlighted with Blue panel is captured the area of "scaffoldA04:20675496-20678125" on ZS11 genome.

Figure S7. QDR against to *B. cinerea* infection is not affected by the magnitude of either BcNEP2 or flg22-induced ROS production. (a) Violin plot illustrating the distributions of lesion sizes belongs to 2 different groups of 30 Low flg22 Responder (Pink) and 30 High flg22 Responder F2 individuals (Purple). (b) Violin plot illustrating the distributions of lesion sizes belongs to 2 different groups of 30 Low BcNEP2 Responder (light blue) and 30 High BcNEP2 Responder F2 individuals (Blue).

Figure S8. Correlation analysis between the 50 nM BcNEP2-induced ROS production results of individual F2 plants from the Ning1 × 7 population and corresponding 20 nM flg22-induced ROS production results. Histogram plots integrated with rug plots of total RLU in response to 50 nM BcNEP2 (upper left) and 20 nM flg22 (lower right), respectively. The scatter plot (lower left) was drawn with LOESS smooth showing the positive correlation between the results. The correlation coefficient value is in the upper right.

Figure S9. Manhattan plots created with corresponded calculations of the Bulk Frequency Ratios of the variants. (a) The highest associated peaks for the High NLP-responsiveness, BFR ratios are calculated between Pool4 and Pool3. 2 753 844 variants (INDELs and SNPs) are plotted along the *x*-axis on the full genome. (b) The highest associated peaks for the High flg22-responsiveness, BFR ratios are calculated between Pool2 and Pool1 Variants are plotted along the *x*-axis on the ZS11 genome. Red line indicates BFR value of 4.

Figure S10. Distribution of the variants on A01 associating with the high NLPinduced ROS production. Manhattan plots created with the calculations of the Bulk Frequency Ratios of the variants. The highest associated peaks for the High NLP-responsiveness, BFR ratios are calculated between Pool4 and Pool3. 139 643 variants (INDELs and SNPs) are plotted along the *x*-axis on the A01 chromosome. Black dashed lines are used to show the boundaries of the peak spread on ~5 Mbp region.

Figure S11. Alignment of *AtBSK1 (AT4G35230.1)* coding sequence (cds) with the cds of its *B. napus* ortholog on A01 chromosome; *BnaA01G0031400ZS*. Genomic locations of *BnaA01G0031400ZS* coding regions are; exon1; scaffoldA01:1744891-1745242, exon2; scaffoldA01:1745318-1745455, exon3; scaffoldA01:1745651-1745785, exon4; scaffoldA01:1745859-1745967, exon5; scaffoldA01:1746093-1746180, exon6; scaffoldA01:1746296-1746486, exon7; scaffoldA01:1746566-1746730, exon8; scaffoldA01:1747318-1747433 and exon9; scaffoldA01:1747498-1747744. Exonic regions were obtained as hits after performing BLAST search (e-value cut off 1e-5) against ZS11 reference genome (Song et al., 2020) using *AT4G35230.1* cds as query. Figure is generated by using *Mview* platform (Maderia et al., 2022; https://doi.org/10.1093/nar/gkac240).

Figure S12. The image of cloned and digested fragments from the mutation region of 8 *bsk1-1* and 8 Col-0 plants. A CAPS marker designed to detect the *bsk1-1* mutation was used to amplify the region of interest. The PCR fragments were obtained and digested with restriction enzyme. As expected, the Col-0 doesn't have a *bsk1-1* mutation in its genome, so it migrates at 82 and 77 base pair (bp). The *bsk1-1* mutation is confirmed by the fragment, which remains undigested by the enzyme and so migrates at 159 bp. The fragments were separated in a 2.4% denatured Agarose gel. 1st row is 100 bp DNA Ladder (NEB #B7025). Corresponding sample names of the lanes are represented in the figure.

Figure S13. Mutation at *bsk1* is not affecting the flg22-induced ROS production. Leaves of the Col0 (wild type), *bsk1-1* mutant lines were treated with 50 nM, 10 nM, 2 nM flg22 incubated with luminol and horseradish peroxidase to detect ROS. Data represent total RLU read over 40 min. Error bars are the standard error of 8 biological replicates.

Figure S14. Histogram plot of depth (DP) and quality (QUAL) values for 3 801 929 variations colour coded based on their locations on the *B. napus* chromosomes. (bin width = 1). (a) Depth – Ningyou1 (b) Depth – Ningyou7 (c) Depth – Pool 1 (d) Depth – Pool 2 **(e)** Depth – Pool 3 **(f)** Depth – Pool 4 **(g)** Quality values of all variants in each corresponded chromosome (bin width = 1).

Table S1. The list of NLP-responsive *B. napus* lines from the diversity set used in AT.

Table S2. Mean and binary BcNEP2-induced ROS production and allele frequencies at loci Cab026058.1:2050:T (A04) and Bo5G145300.1:259:T (C05) for each of the *B. napus* genotype.

Table S3. List of 250 genes in linkage disequilibrium with marker Cab026058.1:2050:T (A04).

Table S4. List of 252 genes in linkage disequilibrium with marker Bo5g145300.1:259:T (C05).

Table S5. BcNEP2-induced ROS production and flg22-induced ROS production values of the pools of 30 F_2 individuals from BSA population.

Table S6. Functional annotation and *A. thaliana* homologues of the genes associated with NLP-responsiveness on Darmor-*bzh* chromosome A09, C04 and C01.

Table S7. KASP primer sequences and their corresponding SNPs.

Table S8. The classification of the SNP effect impacts.

Table S9. Annotation and effect prediction of 1170 variants on A04 have predicted effect on 245 genes with their corresponding locations on Darmor-*bzh* genome.

Table S10. Functional annotation and *A. thaliana* homologues of the genes associated with NLP-responsiveness on Darmor-*bzh* chromosome A04.

Table S11. Annotation and effect prediction of 3938 variants on A04 have predicted effect on 391 genes with their corresponding locations on ZS11 genome.

Table S12. *A. thaliana* homologues of 391 genes associated with NLP-responsiveness on ZS11 chromosome A04.

Table S13. Annotation and effect prediction of 40 variants on A02 have predicted effect on 64 genes with their corresponding locations on ZS11 genome.

Table S14. *A. thaliana* homologues of 64 genes associated with high flg22-induced ROS response phenotype on ZS11 chromosome A02.

Table S15. *A. thaliana* homologues of 328 genes out of 418 genes associated with high BcNEP2-responsiveness on ZS11 chromosome A01.

Table S16. Annotation and effect prediction of 131 variants on A01 have predicted effect on BnaA01G0031400ZS with their corresponding locations on ZS11 genome.

Table S17. Primer sequences used in the genotyping.

Table S18. Annotation and effect prediction of SNPs used in the KASP assay.

REFERENCES

Albert, I., **Böhm, H.**, **Albert, M.**, **Feiler, C.E.**, **Imkampe, J.**, **Wallmeroth, N.** ***et al.*** (2015) An RLP23-SOBIR1-BAK1 complex mediates NLP-triggered immunity. *Nature Plants*, **1**(October), 1–9. Available from: https://doi.org/10.1038/nplants.2015.140

Bhatti, A.A., **Haq, S.** & **Bhat, R.A.** (2017) Actinomycetes benefaction role in soil and plant health. *Microbial Pathogenesis*, **111**, 458–467. Available from: https://doi.org/10.1016/j.micpath.2017.09.036

Bradbury, P.J., **Zhang, Z.**, **Kroon, D.E.**, **Casstevens, T.M.**, **Ramdoss, Y.** & **Buckler, E.S.** (2007) TASSEL: software for association mapping of complex traits in diverse samples. *Bioinformatics (Oxford, England)*, **23**(19), 2633–2635. Available from: https://doi.org/10.1093/BIOINFORMATICS/BTM308

Broman, K.W., **Wu, H.**, **Sen, Ś.** & **Churchill, G.A.** (2003) R/qtl: QTL mapping in experimental crosses. *Bioinformatics*, **19**, 889–890.

Chalhoub, B., **Denoeud, F.**, **Liu, S.**, **Parkin, I.A.P.**, **Tang, H.**, **Wang, X.** ***et al.*** (2014) Early allopolyploid evolution in the post-neolithic Brassica napus oilseed genome. *Science*, **345**(6199), 950–953. Available from: https://doi.org/10.1126/science.1253435

Cingolani, P., **Patel, V.M.**, **Coon, M.**, **Nguyen, T.**, **Land, S.J.**, **Ruden, D.M.** ***et al.*** (2012) Using Drosophila melanogaster as a model for genotoxic chemical mutational studies with a new program, SnpSift. *Frontiers in Genetics*, **3** (MAR), 35. Available from: https://doi.org/10.3389/fgene.2012.00035

Cingolani, P., **Platts, A.**, **Wang, L.L.**, **Coon, M.**, **Nguyen, T.** & **Wang, L.** (2012) A program for annotating and predicting the effects of single nucleotide polymorphisms, SnpEff: SNPs in the genome of Drosophila melanogaster strain w1118; iso-2; iso-3. *Fly (Austin)*, **6**(2), 80–92. Available from: https://doi.org/10.1016/S1877-1203(13)70353-7

Dakouri, A., **Lamara, M.**, **Karim, M.M.**, **Wang, J.**, **Chen, Q.**, **Gossen, B.D.** ***et al.*** (2021) Identification of resistance loci against new pathotypes of Plasmodiophora brassicae in Brassica napus based on genome-wide association mapping. *Scientific Reports*, **11**(1), 1–11. Available from: https://doi.org/10.1038/s41598-021-85836-9

Danecek, P., **Auton, A.**, **Abecasis, G.**, **Albers, C.A.**, **Banks, E.**, **DePristo, M.A.** ***et al.*** (2011) The variant call format and VCFtools. *Bioinformatics*, **27**(15), 2156–2158. Available from: https://doi.org/10.1093/bioinformatics/btr330

Danecek, P., **Bonfield, J.K.**, **Liddle, J.**, **Marshall, J.**, **Ohan, V.**, **Pollard, M.O.** ***et al.*** (2021) Twelve years of SAMtools and BCFtools. *GigaScience*, **10**(2), 1–4. Available from: https://doi.org/10.1093/gigascience/giab008

Durinck, S., **Moreau, Y.**, **Kasprzyk, A.**, **Davis, S.**, **De Moor, B.**, **Brazma, A.** ***et al.*** (2005) BioMart and bioconductor: a powerful link between biological databases and microarray data analysis. *Bioinformatics*, **21**(16), 3439–3440. Available from: https://doi.org/10.1093/bioinformatics/bti525

Durinck, S., **Spellman, P.T.**, **Birney, E.** & **Huber, W.** (2009) Mapping identifiers for the integration of genomic datasets with the R/Bioconductor package biomaRt. *Nature Protocols*, **4**(8), 1184–1191. Available from: https://doi.org/10.1038/nprot.2009.97

Felix, G., **Duran, J.D.**, **Volko, S.** & **Boller, T.** (1999) Plants have a sensitive perception system for the most conserved domain of bacterial flagellin. *The Plant Journal*, **18**(3), 265–276. Available from: https://doi.org/10.1046/j.1365-313x.1999.00265.x

Fell, H., **Muthayil Ali, A.**, **Wells, R.**, **Mitrousia, G.K.**, **Woolfenden, H.**, **Schoonbeek, H.J.** ***et al.*** (2022) Novel gene loci associated with susceptibility or cryptic quantitative resistance to *Pyrenopeziza brassicae* in *Brassica napus*. *Theoretical and Applied Genetics*, **136**, 71. Available from: https://doi.org/10.1007/s00122-023-04243-y

Garrison, E. & **Marth, G.** (2012) *Haplotype-based variant detection from short-read sequencing*. 1–9. Available from: http://arxiv.org/abs/1207.3907 [Accessed 12th February 2020].

Gómez-Gómez, L. & **Boller, T.** (2000) FLS2: an LRR receptor-like kinase involved in the perception of the bacterial elicitor flagellin in Arabidopsis. *Molecular Cell*, **5**(6), 1003–1011. Available from: https://doi.org/10.1016/s1097-2765(00)80265-8

Havlickova, L., **He, Z.**, **Wang, L.**, **Langer, S.**, **Harper, A.L.**, **Kaur, H.** ***et al.*** (2018) Validation of an updated associative transcriptomics platform for the polyploid crop species *Brassica napus* by dissection of the genetic architecture of erucic acid and tocopherol isoform variation in seeds. *Plant Journal*, **93** (1), 181–192. Available from: https://doi.org/10.1111/tpj.13767

Huang, M., **Liu, X.**, **Zhou, Y.**, **Summers, R.M.** & **Zhang, Z.** (2019) BLINK: a package for the next level of genome-wide association studies with both individuals and markers in the millions. *GigaScience*, **8**(2), giy154. Available from: https://doi.org/10.1093/GIGASCIENCE/GIY154

Kim, D., **Paggi, J.M.**, **Park, C.**, **Bennett, C.** & **Salzberg, S.L.** (2019) Graph-based genome alignment and genotyping with HISAT2 and HISAT-genotype. *Nature Biotechnology*, **37**(8), 907–915. Available from: https://doi.org/10.1038/s41587-019-0201-4

Kunze, G., **Zipfel, C.**, **Robatzek, S.**, **Niehaus, K.**, **Boller, T.** & **Felix, G.** (2004) The N terminus of bacterial elongation factor Tu elicits innate immunity in Arabidopsis plants. *Plant Cell*, **16**(12), 3496–3507. Available from: https://doi.org/10.1105/tpc.104.026765

Li, H. & **Durbin, R.** (2010) Fast and accurate long-read alignment with Burrows-Wheeler transform. *Bioinformatics*, **26**(5), 589–595. Available from: https://doi.org/10.1093/bioinformatics/btp698

Lipka, A.E., **Tian, F.**, **Wang, Q.**, **Peiffer, J.**, **Li, M.**, **Bradbury, P.J.** ***et al.*** (2012) GAPIT: genome association and prediction integrated tool. *Bioinformatics (Oxford, England)*, **28**(18), 2397–2399. Available from: https://doi.org/10.1093/BIOINFORMATICS/BTS444

Liu, X., **Huang, M.**, **Fan, B.**, **Buckler, E.S.** & **Zhang, Z.** (2016) Iterative usage of fixed and random effect models for powerful and efficient genome-wide association studies. *PLoS Genetics*, **12**(2), e1005767. Available from: https://doi.org/10.1371/journal.pgen.1005767

Lloyd, S.R. (2014) *Mapping PAMP responses and disease resistance in Brassicas (issue March)*. Doctoral thesis, University of East Anglia, Norwich, UK.

McLoughlin, A.G., **Wytinck, N.**, **Walker, P.L.**, **Girard, I.J.**, **Rashid, K.Y.**, **De Kievit, T.** ***et al.*** (2018) Identification and application of exogenous dsRNA confers plant protection against Sclerotinia sclerotiorum and Botrytis cinerea. *Scientific Reports*, **8**(1), 1–14. Available from: https://doi.org/10.1038/s41598-018-25434-4

Michelmore, R.W., **Paran, I.** & **Kesseli, R.V.** (1991) Identification of markers linked to disease-resistance genes by bulked segregant analysis: a rapid method to detect markers in specific genomic regions by using segregating populations. *Proceedings of the National Academy of Sciences of the United States of America*, **88**(21), 9828–9832. Available from: https://doi.org/10.1073/pnas.88.21.9828

Nichols, B. (2022) bsnichols/GAGA: GAGA v1.0. Available from: https://doi.org/10.5281/ZENODO.7034543 [Accessed 8th November 2022].

Nie, H., **Wu, Y.**, **Yao, C.** & **Tang, D.** (2011) Suppression of edr2-mediated powdery mildew resistance, cell death and ethylene-induced senescence by mutations in ALD1 in Arabidopsis. *Journal of Genetics and Genomics*, **38**(4), 137–148. Available from: https://doi.org/10.1016/j.jgg.2011.03.001

Ono, E., **Mise, K.** & **Takano, Y.** (2020) RLP23 is required for Arabidopsis immunity against the grey mould pathogen *Botrytis cinerea*. *Scientific Reports*, **10**(1), 1–12. Available from: https://doi.org/10.1038/s41598-020-70485-1

Oome, S., **Raaymakers, T.M.**, **Cabral, A.**, **Samwel, S.**, **Böhm, H.**, **Albert, I.** ***et al.*** (2014) Nep1-like proteins from three kingdoms of life act as a microbe-associated molecular pattern in Arabidopsis. *Proceedings of the National Academy of Sciences of the United States of America*, **111**(47), 16955–16960. Available from: https://doi.org/10.1073/pnas.1410031111

Oome, S. & **Van den Ackerveken, G.** (2014) Comparative and functional analysis of the widely occurring family of Nep1-like proteins. *Molecular Plant-Microbe Interactions*, **27**(10), 1081–1094. Available from: https://doi.org/10.1094/mpmi-04-14-0118-r

Raboanatahiry, N., **Li, H.**, **Yu, L.** & **Li, M.** (2021) Rapeseed (*Brassica napus*): processing, utilization, and genetic improvement. *Agronomy*, **11**(9), 1776. Available from: https://doi.org/10.3390/agronomy11091776

Ramirez-Gonzalez, R.H., **Segovia, V.**, **Bird, N.**, **Fenwick, P.**, **Holdgate, S.**, **Berry, S.** ***et al.*** (2015) RNA-Seq bulked segregant analysis enables the identification of high-resolution genetic markers for breeding in hexaploid wheat. *Plant Biotechnology Journal*, **13**(5), 613–624. Available from: https://doi.org/10.1111/pbi.12281

Ramirez-Gonzalez, R.H., **Uauy, C.** & **Caccamo, M.** (2015) PolyMarker: a fast polyploid primer design pipeline. *Bioinformatics*, **31**(12), 2038–2039. Available from: https://doi.org/10.1093/bioinformatics/btv069

Robinson, J.T., **Thorvaldsdóttir, H.**, **Winckler, W.**, **Guttman, M.**, **Lander, E.S.**, **Getz, G.** ***et al.*** (2011) Integrative genomics viewer. *Nature Biotechnology*, **29**(1), 24–26. Available from: https://doi.org/10.1038/nbt.1754

Roy, J., **Shaikh, T.M.**, **del Río Mendoza, L.**, **Hosain, S.**, **Chapara, V.** & **Rahman, M.** (2021) Genome-wide association mapping and genomic prediction for adult stage sclerotinia stem rot resistance in *Brassica napus* (L) under field environments. *Scientific Reports*, **11**(1), 1–18. Available from: https://doi.org/10.1038/s41598-021-01272-9

Schmidt, R., **Acarkan, A.** & **Boivin, K.** (2001) Comparative structural genomics in the Brassicaceae family. *Plant Physiology and Biochemistry*, **39** (3–4), 253–262. Available from: https://doi.org/10.1016/S0981-9428(01)01239-6

Schoonbeek, H., **Del Sorbo, G.** & **De Waard, M.A.** (2001) The ABC transporter BcatrB affects the sensitivity of Botrytis cinerea to the phytoalexin resveratrol and the fungicide fenpiclonil. *Molecular Plant-Microbe Interactions*, **14**(4), 562–571. Available from: https://doi.org/10.1094/MPMI.2001.14.4.562

Schoonbeek, H.-J., **Yalcin, H.A.**, **Burns, R.**, **Taylor, R.E.**, **Casey, A.**, **Holt, S.** ***et al.*** (2022) Necrosis and ethylene-inducing-like peptide patterns from crop pathogens induce differential responses within seven brassicaceous species. *Plant Pathology*, **00**, 1–13. Available from: https://doi.org/10.1111/ppa.13615

Seidl, M.F. & **Van den Ackerveken, G.** (2019) Activity and phylogenetics of the broadly occurring family of microbial Nep1-like proteins. *Annual Review of Phytopathology*, **57**(1), 367–386. Available from: https://doi.org/10.1146/annurev-phyto-082718-100054

Shi, H., **Shen, Q.**, **Qi, Y.**, **Yan, H.**, **Nie, H.**, **Chen, Y.** ***et al.*** (2013) BR-signaling kinase1 physically associates with flagellin SENSING2 and regulates plant innate immunity in Arabidopsis. *Plant Cell*, **25**(3), 1143–1157. Available from: https://doi.org/10.1105/tpc.112.107904

Song, J.M., **Guan, Z.**, **Hu, J.**, **Guo, C.**, **Yang, Z.**, **Wang, S.** ***et al.*** (2020) Eight high-quality genomes reveal pan-genome architecture and ecotype differentiation of Brassica napus. *Nature Plants*, **6**(1), 34–45. Available from: https://doi.org/10.1038/s41477-019-0577-7

Storey, J.D. (2011) False discovery rate. In: Lovric, M. (Ed.) *International Encyclopedia of Statistical Science*. Berlin, Heidelberg: Springer, pp. 504–508. Available from: https://doi.org/10.1007/978-3-642-04898-2_248

Takagi, H., **Abe, A.**, **Yoshida, K.**, **Kosugi, S.**, **Natsume, S.**, **Mitsuoka, C.** ***et al.*** (2013) QTL-seq: rapid mapping of quantitative trait loci in rice by whole genome resequencing of DNA from two bulked populations. *Plant Journal*, **74**(1), 174–183. Available from: https://doi.org/10.1111/tpj.12105

Tekaia, F. & **Latgé, J.P.** (2005) Aspergillus fumigatus: saprophyte or pathogen? *Current Opinion in Microbiology*, **8**(4), 385–392. Available from: https://doi.org/10.1016/j.mib.2005.06.017

Trick, M., **Adamski, N.M.**, **Mugford, S.G.**, **Jiang, C.C.**, **Febrer, M.** & **Uauy, C.** (2012) Combining SNP discovery from next-generation sequencing data with bulked segregant analysis (BSA) to fine-map genes in polyploid wheat. *BMC Plant Biology*, **12**, 14. Available from: https://doi.org/10.1186/1471-2229-12-14

Tudor, E.H., **Jones, D.M.**, **He, Z.**, **Bancroft, I.**, **Trick, M.**, **Wells, R.** ***et al.*** (2020) QTL-seq identifies BnaFT.A02 and BnaFLC.A02 as candidates for variation in vernalization requirement and response in winter oilseed rape (*Brassica napus*). *Plant Biotechnology Journal*, **18**(12), 2466–2481. Available from: https://doi.org/10.1111/pbi.13421

Vetter, M., **Karasov, T.L.** & **Bergelson, J.** (2016) Differentiation between MAMP triggered defenses in *Arabidopsis thaliana*. *PLoS Genetics*, **12**(6), e1006068. Available from: https://doi.org/10.1371/journal.pgen.1006068

Vetter, M., **Kronholm, I.**, **He, F.**, **Häweker, H.**, **Reymond, M.**, **Bergelson, J.** ***et al.*** (2012) Flagellin perception varies quantitatively in *Arabidopsis thaliana* and its relatives. *Molecular Biology and Evolution*, **29**(6), 1655–1667. Available from: https://doi.org/10.1093/molbev/mss011

Wan, W.L., **Zhang, L.**, **Pruitt, R.**, **Zaidem, M.**, **Brugman, R.**, **Ma, X.** ***et al.*** (2019) Comparing Arabidopsis receptor kinase and receptor protein-mediated immune signaling reveals BIK1-dependent differences. *New Phytologist*, **221**(4), 2080–2095. Available from: https://doi.org/10.1111/nph.15497

Wang, H., **Cheng, H.**, **Wang, W.**, **Liu, J.**, **Hao, M.**, **Mei, D.** ***et al.*** (2016) Identification of BnaYUCCA6 as a candidate gene for branch angle in Brassica napus by QTL-seq. *Scientific Reports*, **6**(December), 1–10. Available from: https://doi.org/10.1038/srep38493

Wang, J. & **Zhang, Z.** (2021) GAPIT version 3: boosting power and accuracy for genomic association and prediction. *Genomics, Proteomics & Bioinformatics*, **19**(4), 629–640. Available from: https://doi.org/10.1016/j.gpb.2021.08.005

Wang, X., **Long, Y.**, **Wang, N.**, **Zou, J.**, **Ding, G.**, **Broadley, M.R.** ***et al.*** (2017) Breeding histories and selection criteria for oilseed rape in Europe and China identified by genome wide pedigree dissection. *Scientific Reports*, **7**(1), 1916. Available from: https://doi.org/10.1038/s41598-017-02188-z

Wickham, H. (2016) *ggplot2: Elegant Graphics for Data Analysis*. Houston, TX: Springer-Verlag New York. ISBN: 978-3-319-24277-4. Available from: https://ggplot2.tidyverse.org [Accessed 23rd May 2020].

Zipfel, C., **Kunze, G.**, **Chinchilla, D.**, **Caniard, A.**, **Jones, J.D.**, **Boller, T.** ***et al.*** (2006) Perception of the bacterial PAMP EF-Tu by the receptor EFR restricts Agrobacterium-mediated transformation. *Cell*, **125**(4), 749–760. Available from: https://doi.org/10.1016/j.cell.2006.03.037

Zou, C., **Wang, P.** & **Xu, Y.** (2016) Bulked sample analysis in genetics, genomics and crop improvement. *Plant Biotechnology Journal*, **14**(10), 1941–1955. Available from: https://doi.org/10.1111/pbi.12559

Zou, J., **Mao, L.**, **Qiu, J.**, **Wang, M.**, **Jia, L.**, **Wu, D.** ***et al.*** (2019) Genome-wide selection footprints and deleterious variations in young Asian allotetraploid rapeseed. *Plant Biotechnology Journal*, **17**(10), 1998–2010. Available from: https://doi.org/10.1111/pbi.13115